Modeling of Air-Conditioner Compressor Single Phase Induction Motor for

Transient Analysis

by

Yuan Liu

A Thesis Presented in Partial Fulfillment
of the Requirements for the Degree
Master of Science

Approved November 2012 by the
Graduate Supervisory Committee:

Vijay Vittal, Chair
John Undrill
Raja Ayyanar

ARIZONA STATE UNIVERSITY

December 2012

ABSTRACT

This thesis presents a new technique to develop an air-conditioner (A/C) compressor single phase induction motor model for use in an electro-magnetic transient program (EMTP) simulation tool. The method developed also has the capability to represent multiple units of the component in a specific three-phase distribution feeder and investigate the phenomenon of fault-induced delayed voltage recovery (FIDVR) and the cause of motor stalling.

The system of differential equations representing the single phase induction motor model is developed and formulated. Implicit backward Euler method is applied to numerically integrate the stator currents that are to be drawn from the electric network. The angular position dependency of the rotor shaft is retained in the inductance matrix associated with the model to accurately capture the dynamics of the motor loads. The equivalent circuit of the new model is interfaced with the electric network in the EMTP. The dynamic response of the motor when subjected to faults at different points on voltage waveform has been studied using the EMTP simulator. The mechanism and the impacts of motor stalling need to be explored with multiple units of the detailed model connected to a realistic three-phase distribution system. The model developed can be utilized to assess and improve the product design of compressor motors by air-conditioner manufacturers. Another critical application of the model would be to examine the impacts of asymmetric transmission faults on distribution systems to investigate and develop mitigation measures for the FIDVR problem.

ACKNOWLEDGEMENTS

I would like to first and foremost express my sincerest gratitude to my advisor, Dr. Vijay Vittal, whose encouragement, guidance and support have motivated me to make significant progress on the research and complete my thesis. I also attribute the success of my Master's degree to Dr. John Undrill for his extensive input on both my research topic and the practical issues associated the phenomenon. I also want to express my gratitude to Dr. Raja Ayyanar for his time and consideration in being a member of my graduate supervisory committee.

I especially want to thank my parents Mr. Peizhong Liu and Mrs. Xiufeng Wang for their support of my higher education. I also would like to thank my friends and roommates who encouraged me.

TABLE OF CONTENTS

LIST OF TABLES

LIST OF FIGURES

NOMENCLATURE

A/C   Air-Conditioner

DC   Direct Current

EMTDC   Electro-Magnetic Transients including Direct Current

EMTP   Electro-Magnetic Transients Program

FIDVR   Fault-Induced Delayed Voltage Recovery

GE   General Electric

GUI   Graphical User Interface

HVDC   High Voltage Direct Current

MVA   Mega Volt Ampere

MVWG   Modeling and Validation Work Group

PSCAD   Power Systems Computer Aided Design

PSLF   Positive Sequence Load Flow

PSS/E   Power System Simulator for Engineering

P-O-W   Point-On-Wave

RTDS   Real Time Digital Simulator

SPIM   Singe Phase Induction Motor

SVC   Static Var Compensator

TSAT   Transient Security Assessment Tool

WECC   Western Electricity Coordinating Council

as   Stator main winding

ar	Rotor main winding
bs	Stator auxiliary winding
br	Rotor auxiliary winding
ccap	Auxiliary winding capacitor
diam	Rotor shaft diameter
E_{thas}	Equivalent Thevenin source of stator main winding
E_{thbs}	Equivalent Thevenin source of stator auxiliary winding
H_r	Polar moment of inertia of the rotor
i_{as}	Current through *as* winding
i_{bs}	Current through *bs* winding
i_{ar}	Current through *ar* winding
i_{br}	Current through *br* winding
length	Rotor shaft length
L_{sat}	Saturated inductance
L_{unsat}	Unsaturated inductance
L_m	Saturated mutual inductance between stator main winding and rotor winding
L_{mu}	Unsaturated mutual inductance between stator main winding and rotor winding
L_s	Leakage inductance of stator main winding or stator auxiliary winding
L_r	Leakage inductance of rotor main winding or rotor auxiliary winding

N	Turns ratio of stator auxiliary winding to stator main winding
r_s	Stator winding resistance
r_{cage}	Rotor cage resistance
rr	Static rotor coil resistance
S	Parabolic form saturation function
S_1	MVA rating of each prototype motor model
S_{total}	Total MVA rating of a group of prototype motors
$scale$	Scaling factor
Δt	Time step
T_e	Electro-magnetic torque
T_{mech}	Mechanical load torque
$Tload$	Friction and windage load coefficient
Tav	Compressor triangular waveform load coefficient
V_{as}	Voltage of *as* winding
V_{bs}	Voltage of *bs* winding
V_{ar}	Voltage of *ar* winding
V_{br}	Voltage of *br* winding
ω	Rotor angular velocity
ω_o	Fundamental angular frequency
Z_{aa}	Shunt impedance of stator main winding equivalent Norton branch

Z_{bb}	Shunt impedance of stator auxiliary winding equivalent Norton branch
λ_{as}	Total flux linkage of as winding
λ_{bs}	Total flux linkage of bs winding
λ_{ar}	Total flux linkage of ar winding
λ_{br}	Total flux linkage of br winding
λ_{am}	Air gap flux linkage with respect to as winding
λ_{bm}	Air gap flux linkage with respect to bs winding
λ_{base}	Base flux linkage
λ_{mpu}	Total flux linkage of as winding and bs winding in per unit
θ	Physical position of rotor winding centerline relative to stator structure

Chapter 1.   INTRODUCTION OF RESEARCH

1.1   Background

Fault-induced delayed voltage recovery (FIDVR) is a phenomenon characterized by the power system voltages remaining at a depressed level for several seconds after a transmission fault is cleared. FIDVR events have been observed in Southern California, Arizona, Texas, Florida, and other southeastern parts of the U.S.

Wide spread stalling of residential single phase air-conditioners is generally regarded to be the main cause of the FIDVR phenomenon. Residential air-conditioners can stall in as short as five cycles if the motor terminal voltage goes below 60% of normal value [1]- [2]. Once a single phase air-conditioner compressor stalls, it is unlikely to restart because the electrical torque cannot overcome the load torque after the fault is cleared. The stalled motor will draw high current until it is tripped off by internally installed cut-off protection. As a consequence the voltages at the distribution system will be depressed due to high currents flowing through the feeder lines. The increased amount of reactive power drawn by the stalled motor loads will further depress the bus voltage on the system. The stalling of up-stream motors in the feeder may aggravate the voltage depression and expedite the stalling of the down-stream motors. Prolonged voltage recovery increases the risk of losing power plants, static var compensators (SVCs), and other rotating machine loads. Degraded voltage also deteriorates the power quality of the grid by leading to dim lighting. The A/C compressor motor is

1

known to have a small inertia constant, which is largely responsible for the "prone-to-stall" characteristics of the SPIM. The simplest solution to the FIDVR problem might seem to be tripping the stalled motors by appropriate means. The primary disadvantage of this solution is the risk of over-voltage raised by tripping the inductive load.

Development of accurate single phase induction motor load models for air-conditioner compressors is critical to study FIDVR events and stalling mechanisms of motors. The Western Electricity Coordinating Council (WECC), modeling and validation working group (MVWG) has initiated the development of new load models. The previous effort made by this group was to represent the air-conditioner compressor motor model in the conventional positive sequence transient stability software packages as a portion of the composite load model. Presently, the composite load model structure developed has successfully been incorporated into PSLF, PSS/E, TSAT and other software packages. Models based on dynamic phasors are also being considered to represent the characteristics of single phase induction motors in more detail. These models are presently under investigation and being incorporated in PSLF.

1.2   Previous work

Early research efforts [1] [3] [4] have dealt with equipment-level modeling and grid-level modeling of single phase induction motor models. It is important to distinguish between grid-level models and equipment-level models. Detailed equipment-level models are suitable for individual component analysis and examination of system response at specific locations. For grid-level studies

2

however, the precision using equipment-level models is typically lost [5]. Simpler models can be formulated to capture the equipment behavior at the grid level. Two different types of single phase induction motor models; performance model and dynamic phasor model have been proposed for years. The performance model [6] represents the effects of motor loads in the form of real and reactive power consumption as a function of voltage and temperature. This model operates in three states: running, stalled and trip-off. The dynamic phasor model is an equipment-level model [5] [7]. The dynamic phasor model is a physical model represented by differential matrix equations. These equations are used to represent the dynamic behavior of individual motors.

1.3   Major objectives of the research

The overall objective of this research is to develop a user-defined single phase induction motor model in the commercial Power System Computer Aided Design (PSCAD) software package and to represent multiple units of that component on a given distribution feeder to study the FIDVR phenomenon.

Recent studies [8] [9] have shown that motor stalling depends on the point on the voltage waveform at which the fault occurs. It has been observed that motors are more likely to stall when the fault is applied at the zero crossing point of its terminal voltage waveform and less likely to stall when the fault is applied at the peak of its terminal voltage waveform. PSCAD has the capability to utilize a small resolution time step (micro-seconds level) and analyze unbalanced faults. Additionally a model designed to be compatible with the PSCAD simulator is a desirable solution to analyze the point-on-wave (P-O-W) performance of single

3

phase induction motor dynamics when the three-phase feeder with multiple units of the motor model coupled at different nodes and different phases is subjected to symmetric or asymmetric voltage contingency at the its head. This study can be conducted on any chosen system once the model is developed and implemented.

PSCAD, also known as PSCAD/EMTDC is a commercial time domain transient simulation environment and study tool. There are two approaches to implement a new user-defined model in PSCAD. Fortran codes can be written to execute the specific functional details of the model if it is defined as a component model. This is the most direct approach to define a desired model because complex component connections are not made. The other approach to represent a desired custom model is to set up a module model. Internally defined circuit elements or logic blocks from the PSCAD master library can be found and placed in the module canvas to achieve the same purpose. Compared to the direct programming method, the module canvas approach is less error prone because numerical problems in component definition by coding can be avoided.

In this research, the single phase induction motor model is programmed into PSCAD as a component model. The research involves the development of a dynamic model and a simulation study to support future investigation of the effect of air-conditioner compressor stalling and its impact on delayed voltage recovery of the distribution system.

1.4   Organization of thesis

The thesis is organized in six chapters. Chapter 1 gives a basic introduction to the research. This chapter contains the background statement, description of previous work and major objectives of the research.

Chapter 2 presents the literature review relating to classical modeling strategies that currently exist.

Chapter 3 deals with mathematical development of the proposed model and electrical interface.

Chapter 4 provides the simulation results of a single custom motor component connected to a node through a distribution transformer.

Chapter 5 details the simulation results of multiple motor units on a representative distribution feeder.

The conclusions and findings from the work are provided in Chapter 6. Ideas for future work are also given in this chapter.

Chapter 2.   LITERATURE REVIEW

The early exploration of a single phase induction motor model consisted of developing an equivalent circuit representation of a running motor. The voltage and flux linkage equations of a single phase induction motor have been formulated for more than a century [10]. By transforming the current and voltage quantities of both the stator and rotor into a common stationary reference frame, the time dependency of mutual inductance with respect to rotor angle can be eliminated. Furthermore, the equivalent circuit interfaces of the stator main winding and stator auxiliary winding can be formulated from the voltage and flux equations described in the new reference frame [10] [11]. With the growth of air-conditioner compressor loads in power systems, the compressor single phase induction motor stalling is a problem of concern. Previously developed single phase models cannot emulate the stalling phenomenon in compressor motors.

Two classical models of air-conditioner motor loads have been developed and utilized in recent years [6]. The performance model has proven to be a good approximation of the air-conditioner load features. This model represents the motor operation in three states: running, stalled and trip-off [12]. The air-conditioner loads are represented by real and reactive power consumption as a function of voltage and temperature. This model assumes that once the voltage drops below a set threshold V_{stall} all motors will stall. A hybrid model is proposed with a state transition diagram to capture other important aspects such as the contactor drop out, contactor reclosing and the thermal overload relay [12]. The

performance model has been implemented in PSLF [6]. The discontinuity that exists from the running mode to stalled mode is not explicitly represented. This lack of detail would be an obstacle for investigating the stalling mechanism from an electro-magnetic transients viewpoint. A simpler approach to include the performance model of the air-conditioner load into a positive sequence simulator for short-term voltage stability study is proposed in [3]. The effective active and reactive power drawn by motor components are determined under normal operating conditions and stalled conditions. The aggregate Mega-Volt-Ampere (MVA) of "prone-to-stall" motor loads and the load power factors under normal operation and stalled mode are the three parameters needed to compute the real and reactive power consumption at the two different conditions. The MVA rating of the motor under stalled mode is scaled by multiplying the per unit locked rotor current (generally 4.0 - 6.0 per unit) to reproduce post-stall characteristics.

According to [1], most residential air-conditioner compressors will experience stalling problems if the supply voltage is depressed below 60% of rated voltage for no less than 5 cycles. For basic single phase induction motors (without auxiliary winding), the pulsating magnetic field produced by the stator winding sinusoidal current can be resolved into two revolving fields of constant magnitude rotating in opposite directions in space, which are forward and backward rotating fields. The forward revolving field is related to positive sequence electrical quantities and the backward field is related to negative sequence variables. The positive sequence and negative sequence equivalent circuits of the single phase induction motor can be constructed separately based

on the two rotating magnetic fields induced by the currents [13]- [14]. The air-conditioner induction motor models simulated in [1] and [2] consider the positive sequence equivalent circuit discussed above. It is assumed that no capacitor-start auxiliary winding is modeled in [1] and [2]. The model has been validated and desirable active and reactive power responses are obtained by applying voltage dip of different levels on the transmission system side.

In recent years, dynamic phasor modeling methods originating in power electronics have become popular. All the electrical variables are represented by time-varying Fourier series instead of using the real stator and rotor winding electrical variables (currents, flux linkages and so on) for analysis. The slowly time-varying Fourier coefficients of those variables are used to formulate dynamical equations. The equivalent circuit is derived considering the effects of forward and backward revolving flux phasors induced by currents [7]. Usually, the fundamental frequency variables are retained and higher order harmonics are neglected in analysis [5]. The orders of harmonics retained are user selected. A balance needs to be struck between computational simplification and modeling accuracy while considering harmonics. This type of model has some advantages in capturing the intrinsic real-time characteristics of single phase machines. The stalling conditions can be reproduced. This is a good example of an equipment-level model. The accuracy however, is degraded if only the fundamental frequency components are considered in the model.

As documented in [15], air-conditioner stalling depends on the point on the voltage waveform at which the fault is applied. This dependence on the point-

8

on-wave complicates modeling of the air-conditioner stalling phenomenon. The different models discussed above are mostly represented in positive sequence simulator packages. The positive sequence simulator packages are known to generally have a 1/4 cycle integration solution time step [6]. This limitation in the integration time step does not allow for the study of point on wave effects. Electro-magnetic transient analysis software packages such as PSCAD do not have such limitations and can be effectively employed to play in voltage dips at different points of sinusoidal waveform [16]. The following chapters detail the proposed procedure for modeling single phase induction motors used in air-conditioner compressors and also provide the results of simulation on various tests.

Chapter 3. MODEL DEVELOPMENT

3.1 Introduction

The common residential air conditioning compressor single phase induction motor is a permanent-split capacitor motor, also referred to as a split phase motor. The capacitor is used to improve the starting and running performance of the single phase induction motors. A capacitor of suitable value is connected in series with the auxiliary coil such that stator auxiliary coil current leads the main coil current by 90 electrical degrees in time phase for maximum starting torque. This becomes an unbalanced two-phase motor if the magnitude of two stator currents is unequal and displaced in space by 90 electrical degrees. With this design, the efficiency and power factor of motor are improved. The schematic of the compressor motor is shown in Figure 3.1.
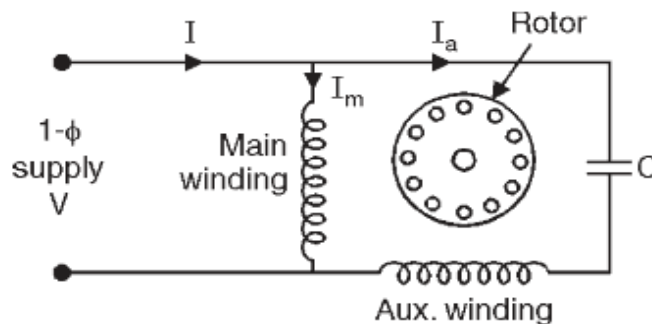
Figure 3.1 Schematic of air-conditioner compressor [16]

3.2 Dynamical equations [8]

The single phase induction motor is modeled at the level of detail to represent electro-magnetic transients. The schematic of the stator and rotor

windings is as shown in Figure 3.2. The mutual inductances between the stator and rotor coils vary sinusoidally with the angular position of the rotor. The number of turns in the two stator coils (*as* and *bs*) are not identical. The capacitor in the stator auxiliary winding (*bs*) is represented explicitly. The flux linkage equations are implemented by the position dependent matrix.
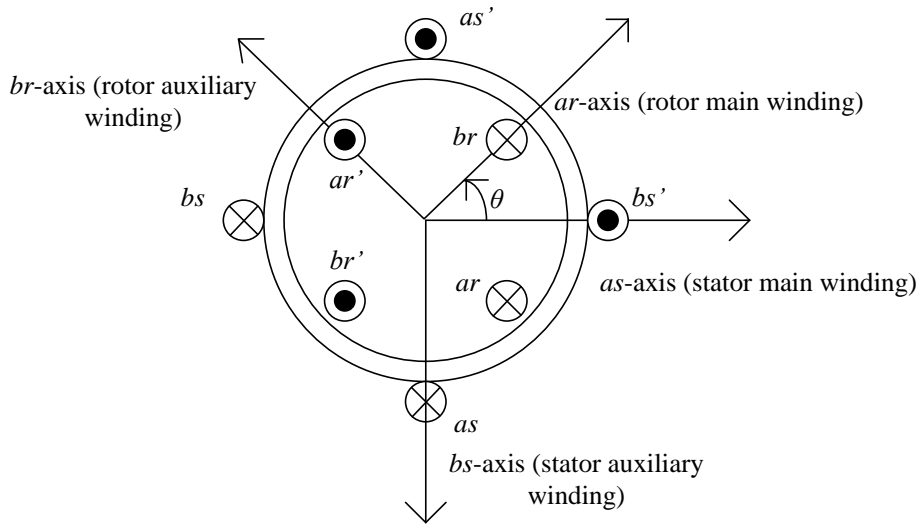
Figure 3.2 Phasor diagram of stator and rotor winding magnetic field

The flux linkage is defined as the product of the current flowing through a coil and the self or mutual inductance with respect to that coil. The direction of flux phasor can be determined by Fleming's right-hand law [10], which is shown in Figure 3.2. In the machine frame, the total flux linkage with respect to one winding combines its leakage flux linkage and the projected components of the mutual flux linkage from other windings.

The flux linkage equations are given as

$$\begin{bmatrix} \lambda_{as} \\ \lambda_{bs} \\ \lambda_{ar} \\ \lambda_{br} \end{bmatrix} = \begin{bmatrix} L_m + L_s & 0 & L_m \cos\theta & L_m \sin\theta \\ 0 & N^2 L_m + L_s & -NL_m \sin\theta & NL_m \cos\theta \\ L_m \cos\theta & -NL_m \sin\theta & L_m + L_r & 0 \\ L_m \sin\theta & NL_m \cos\theta & 0 & L_m + L_r \end{bmatrix} \begin{bmatrix} i_{as} \\ i_{bs} \\ i_{ar} \\ i_{br} \end{bmatrix} \tag{3.1}$$

In (3.1), L_s is the saturated leakage inductance of stator winding (winding *as* or *bs*). L_m is the saturated mutual inductance between the stator main winding (*as*) and the rotor winding. *N* is the turns ratio of the stator auxiliary winding (*bs*) to the stator main winding (*as*). The angle θ is the physical position of the rotor winding centerline relative to the stator structure. Notice that the rotor quantities have already been referred to the stator winding relative to the main winding ratio.

Differentiating (3.1) with respect to time gives

$$\begin{bmatrix} \dfrac{d\lambda_{as}}{dt} \\ \dfrac{d\lambda_{bs}}{dt} \\ \dfrac{d\lambda_{ar}}{dt} \\ \dfrac{d\lambda_{br}}{dt} \end{bmatrix} = \mathbf{Lrs} \begin{bmatrix} \dfrac{di_{as}}{dt} \\ \dfrac{di_{bs}}{dt} \\ \dfrac{di_{ar}}{dt} \\ \dfrac{di_{br}}{dt} \end{bmatrix} + \mathbf{Ars} \begin{bmatrix} i_{as} \\ i_{bs} \\ i_{ar} \\ i_{br} \end{bmatrix} \tag{3.2}$$

where **Lrs** is the inductance matrix in (3.1) and

$$\mathbf{Ars} = \begin{bmatrix} 0 & 0 & -\omega L_m \sin\theta & \omega L_m \cos\theta \\ 0 & 0 & -\omega NL_m \cos\theta & -\omega NL_m \sin\theta \\ -\omega L_m \sin\theta & -\omega NL_m \cos\theta & 0 & 0 \\ \omega L_m \cos\theta & -\omega NL_m \sin\theta & 0 & 0 \end{bmatrix} \tag{3.3}$$

The inductances in the above matrices are varied as a function of the flux in order to represent saturation of the stator and rotor iron. This variation is approximated as follows

12

$$\lambda_{mpu} = \frac{\sqrt{\lambda_{as}^2 + \lambda_{bs}^2}}{\lambda_{base}} \qquad (3.4)$$

$$L_{sat} = \frac{L_{unsat}}{1 + S(\lambda_{mpu})} \qquad (3.5)$$

where S is the standard parabolic form saturation function defined by its values at nominal flux and 1.2 times nominal flux, S (1.0) and S (1.2). The magnetizing curve and the definition of the saturation function are illustrated in Figure 3.3.
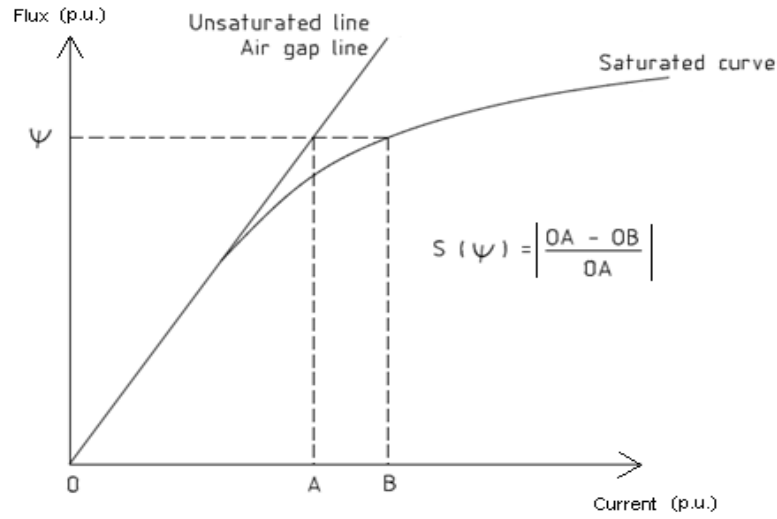
Figure 3.3 Definition of magnetic saturation function [17]

Rotor windings are usually short circuited. Thus V_{ar} and V_{br} are zero. The standard differential equations relating flux, voltage, and current are then given by

$$\frac{d\lambda_{as}}{dt} = V_{as} - r_s i_{as} \qquad (3.6)$$

$$\frac{d\lambda_{bs}}{dt} = V_{bs} - r_s i_{bs} \qquad (3.7)$$

$$\frac{d\lambda_{ar}}{dt} = -r_{cage} i_{ar} \qquad (3.8)$$

$$\frac{d\lambda_{br}}{dt} = -r_{cage}i_{br} \tag{3.9}$$

where r_s is the stator winding resistance and r_{cage} is the rotor cage resistance.

The effective resistance of the rotor is a function of the frequency of rotor currents and hence of rotor speed. The variation of rotor resistance is approximated as

$$r_{cage} = rr\left(5.0 - 4.0\frac{\omega}{\omega_o}\right) \quad \omega < \omega_o \tag{3.10}$$

$$r_{cage} = rr \quad \omega \geq \omega_o \tag{3.11}$$

where rr is the static rotor coil resistance.

The stator and rotor flux linkages are calculated by (3.1). The air gap flux, as needed to calculate torque, is then obtained by

$$\lambda_{am} = \lambda_{as} - L_s i_{as} \tag{3.12}$$

$$\lambda_{bm} = \lambda_{bs} - N^2 L_s i_{bs} \tag{3.13}$$

The electro-magnetic torque is given by

$$T_e = \lambda_{am}(-i_{ar}\sin\theta + i_{br}\cos\theta) - \lambda_{bm}(i_{ar}\cos\theta + i_{br}\sin\theta) \tag{3.14}$$

The motion of the rotor and variation of the angle describing mutual inductances are described by

$$\frac{d\omega}{dt} = \frac{T_e - T_{mech}}{H_r} \tag{3.15}$$

$$\frac{d\theta}{dt} = \omega \tag{3.16}$$

14

in which H_r is the polar moment of inertia of the rotor and T_{mech} is mechanical load torque.

$$H_r = 7800 * \left(\frac{\pi}{32} \right) * length * diam^4 \tag{3.17}$$

where *length* is rotor shaft length in meters and *diam* is rotor shaft diameter in meters.

3.3 Derivation of Norton equivalent expressions

In reality, the two stator windings provide the direct interface to the electric network. The start-up capacitor connected in series with the auxiliary winding is placed externally and incorporated into the electric network at the point of motor interconnection to the network. This section of the work is focused on developing the internal equivalent circuit of the single phase induction motor interfaced to the external system.

For simplification purpose, (3.1) can be written as

$$\begin{bmatrix} \lambda_{abs} \\ \lambda_{abr} \end{bmatrix} = \begin{bmatrix} \mathbf{L}_{ss} & \mathbf{L}_{sr} \\ (\mathbf{L}_{sr})^{\mathbf{T}} & \mathbf{L}_{rr} \end{bmatrix} \begin{bmatrix} \mathbf{i}_{abs} \\ \mathbf{i}_{abr} \end{bmatrix} \tag{3.18}$$

where

$$\mathbf{L}_{ss} = \begin{bmatrix} L_m + L_s & 0 \\ 0 & N^2 L_m + L_s \end{bmatrix} \tag{3.19}$$

$$\mathbf{L}_{rr} = \begin{bmatrix} L_m + L_r & 0 \\ 0 & L_m + L_r \end{bmatrix} \tag{3.20}$$

$$\mathbf{L}_{sr} = \begin{bmatrix} L_m \cos\theta & L_m \sin\theta \\ -N L_m \sin\theta & N L_m \cos\theta \end{bmatrix} \tag{3.21}$$

15

Expressing (3.6) through (3.9) in block matrix form

$$\begin{bmatrix} \mathbf{v}_{abs} \\ \mathbf{v}_{abr} \end{bmatrix} = \begin{bmatrix} \mathbf{r}_{ss} & \mathbf{0} \\ \mathbf{0} & \mathbf{r}_{rr} \end{bmatrix} \begin{bmatrix} \mathbf{i}_{abs} \\ \mathbf{i}_{abr} \end{bmatrix} + \frac{d}{dt} \begin{bmatrix} \lambda_{abs} \\ \lambda_{abr} \end{bmatrix} \qquad (3.22)$$

in which

$$\mathbf{r}_{ss} = \begin{bmatrix} r_s & 0 \\ 0 & r_s \end{bmatrix} \qquad (3.23)$$

$$\mathbf{r}_{rr} = \begin{bmatrix} r_{cage} & 0 \\ 0 & r_{cage} \end{bmatrix} \qquad (3.24)$$

$$\mathbf{v}_{abr} = \mathbf{0} \qquad (3.25)$$

Substitute (3.18) into (3.22)

$$\begin{bmatrix} \mathbf{v}_{abs} \\ \mathbf{v}_{abr} \end{bmatrix} = \begin{bmatrix} \mathbf{r}_{ss} & \mathbf{0} \\ \mathbf{0} & \mathbf{r}_{rr} \end{bmatrix} \begin{bmatrix} \mathbf{i}_{abs} \\ \mathbf{i}_{abr} \end{bmatrix} + \frac{d}{dt} \left(\begin{bmatrix} \mathbf{L}_{ss} & \mathbf{L}_{sr} \\ \left(\mathbf{L}_{sr} \right)^{\mathrm{T}} & \mathbf{L}_{rr} \end{bmatrix} \begin{bmatrix} \mathbf{i}_{abs} \\ \mathbf{i}_{abr} \end{bmatrix} \right) \qquad (3.26)$$

$$\begin{bmatrix} \mathbf{v}_{abs} \\ \mathbf{v}_{abr} \end{bmatrix} = \begin{bmatrix} \mathbf{r}_{ss} & \mathbf{0} \\ \mathbf{0} & \mathbf{r}_{rr} \end{bmatrix} \begin{bmatrix} \mathbf{i}_{abs} \\ \mathbf{i}_{abr} \end{bmatrix} + \frac{d}{dt} \left(\begin{bmatrix} \mathbf{L}_{ss} & \mathbf{L}_{sr} \\ \left(\mathbf{L}_{sr} \right)^{\mathrm{T}} & \mathbf{L}_{rr} \end{bmatrix} \right) \begin{bmatrix} \mathbf{i}_{abs} \\ \mathbf{i}_{abr} \end{bmatrix} + \begin{bmatrix} \mathbf{L}_{ss} & \mathbf{L}_{sr} \\ \left(\mathbf{L}_{sr} \right)^{\mathrm{T}} & \mathbf{L}_{rr} \end{bmatrix} \frac{d}{dt} \begin{bmatrix} \mathbf{i}_{abs} \\ \mathbf{i}_{abr} \end{bmatrix}$$

$$(3.27)$$

Discretize (3.27) and apply implicit Euler integration method

$$\begin{bmatrix} \mathbf{V}_{abs} \\ \mathbf{V}_{abr} \end{bmatrix} = \mathbf{R} \begin{bmatrix} \mathbf{I}_{abs}(t) \\ \mathbf{I}_{abr}(t) \end{bmatrix} + \mathbf{Ars} \begin{bmatrix} \mathbf{I}_{abs}(t) \\ \mathbf{I}_{abr}(t) \end{bmatrix} + \mathbf{Lrs} \frac{1}{\Delta t} \left(\begin{bmatrix} \mathbf{I}_{abs}(t) \\ \mathbf{I}_{abr}(t) \end{bmatrix} - \begin{bmatrix} \mathbf{I}_{abs}(t - \Delta t) \\ \mathbf{I}_{abr}(t - \Delta t) \end{bmatrix} \right)$$

$$(3.28)$$

$$\begin{bmatrix} \mathbf{V}_{abs} \\ \mathbf{V}_{abr} \end{bmatrix} = \left(\mathbf{R} + \mathbf{Ars} + \frac{\mathbf{Lrs}}{\Delta t} \right) \begin{bmatrix} \mathbf{I}_{abs}(t) \\ \mathbf{I}_{abr}(t) \end{bmatrix} + \frac{\mathbf{Lrs}}{\Delta t} \left(- \begin{bmatrix} \mathbf{I}_{abs}(t - \Delta t) \\ \mathbf{I}_{abr}(t - \Delta t) \end{bmatrix} \right) \qquad (3.29)$$

in which

$$\mathbf{R} = \begin{bmatrix} \mathbf{r}_{ss} & \mathbf{0} \\ \mathbf{0} & \mathbf{r}_{rr} \end{bmatrix} = \begin{bmatrix} r_s & 0 & 0 & 0 \\ 0 & r_s & 0 & 0 \\ 0 & 0 & r_{cage} & 0 \\ 0 & 0 & 0 & r_{cage} \end{bmatrix} \qquad (3.30)$$

$$\mathbf{Ars} = \frac{d}{dt}\begin{bmatrix} \mathbf{L}_{ss} & \mathbf{L}_{sr} \\ (\mathbf{L}_{sr})^T & \mathbf{L}_{rr} \end{bmatrix} \qquad (3.31)$$

$$\mathbf{Lrs} = \begin{bmatrix} \mathbf{L}_{ss} & \mathbf{L}_{sr} \\ (\mathbf{L}_{sr})^T & \mathbf{L}_{rr} \end{bmatrix} \qquad (3.32)$$

where **Lrs** and **Ars** are also defined in (3.1) and (3.3).

In the simulation process $\mathbf{I}_{abs}(t - \Delta t)$ and $\mathbf{I}_{abr}(t - \Delta t)$ are known current vectors from the last completed time step. $\mathbf{V}_{abs}$ is the instantaneous stator winding voltage vector obtained from the electric network solution. $\mathbf{I}_{abs}(t)$ and $\mathbf{I}_{abr}(t)$ are current vectors to be determined in the time step being executed.

Equation (3.29) can be written as

$$\begin{bmatrix} \mathbf{V}_{abs} \\ \mathbf{V}_{abr} \end{bmatrix} = \begin{bmatrix} \mathbf{Z}_{ss} & \mathbf{Z}_{sr} \\ \mathbf{Z}_{rs} & \mathbf{Z}_{rr} \end{bmatrix}\begin{bmatrix} \mathbf{I}_{abs}(t) \\ \mathbf{I}_{abr}(t) \end{bmatrix} + \begin{bmatrix} \mathbf{V}_{ts}(t - \Delta t) \\ \mathbf{V}_{tr}(t - \Delta t) \end{bmatrix} \qquad (3.33)$$

where

$$\begin{bmatrix} \mathbf{Z}_{ss} & \mathbf{Z}_{sr} \\ \mathbf{Z}_{rs} & \mathbf{Z}_{rr} \end{bmatrix} = \mathbf{R} + \mathbf{Ars} + \frac{\mathbf{Lrs}}{\Delta t} \qquad (3.34)$$

is a 4 x4 system Thevenin equivalent matrix.

$$\begin{bmatrix} \mathbf{V}_{ts}(t - \Delta t) \\ \mathbf{V}_{tr}(t - \Delta t) \end{bmatrix} = \frac{\mathbf{Lrs}}{\Delta t}\left(- \begin{bmatrix} \mathbf{I}_{abs}(t - \Delta t) \\ \mathbf{I}_{abr}(t - \Delta t) \end{bmatrix} \right) \qquad (3.35)$$

is a 4 x 1 system Thevenin equivalent history voltage vector.

The rotor winding is always short circuited. Thus $\mathbf{V_{abr}} = \mathbf{0}$ and the second row of (3.33) can be expressed as

$$\mathbf{I_{abr}(t)} = -\mathbf{Z_{rr}^{-1}}\left[\mathbf{Z_{rs}I_{abs}(t)} + \mathbf{V_{tr}(t - \Delta t)}\right] \tag{3.36}$$

Substituting (3.36) into the 1st row of (3.33), the stator winding voltage vector can be obtained as

$$\mathbf{V_{abs}} = \left(\mathbf{Z_{ss}} - \mathbf{Z_{sr}Z_{rr}^{-1}Z_{rs}}\right)\mathbf{I_{abs}(t)} - \mathbf{Z_{sr}Z_{rr}^{-1}V_{tr}(t - \Delta t)} + \mathbf{V_{ts}(t - \Delta t)}$$

$$\tag{3.37}$$

Equation (3.37) can be expanded as a 2-dimensional matrix equation and simplified to be a classical Thevenin equivalent expression.

$$\begin{bmatrix} V_{as} \\ V_{bs} \end{bmatrix} = \begin{bmatrix} Z_{aa} & Z_{ab} \\ Z_{ba} & Z_{bb} \end{bmatrix}\begin{bmatrix} I_{as}(t) \\ I_{bs}(t) \end{bmatrix} + \begin{bmatrix} E_{thas}(t - \Delta t) \\ E_{thbs}(t - \Delta t) \end{bmatrix} \tag{3.38}$$

in which

$$\mathbf{Z_{th}} = \begin{bmatrix} Z_{aa} & Z_{ab} \\ Z_{ba} & Z_{bb} \end{bmatrix} = \mathbf{Z_{ss}} - \mathbf{Z_{sr}Z_{rr}^{-1}Z_{rs}} \tag{3.39}$$

is a 2 x 2 matrix.

$$\begin{bmatrix} E_{thas}(t - \Delta t) \\ E_{thbs}(t - \Delta t) \end{bmatrix} = -\mathbf{Z_{sr}Z_{rr}^{-1}V_{tr}(t - \Delta t)} + \mathbf{V_{ts}(t - \Delta t)} \tag{3.40}$$

is a 2 x 1 vector.

Matrix operations are then performed to prove that the off-diagonal elements of $\mathbf{Z_{th}}$ are zeros. The physical reasoning behind this result is that the stator main winding and stator auxiliary winding are electrically decoupled when represented as Thevenin equivalent or alternatively as Norton equivalent branches at the current time instant. The interaction between two stator windings and

18

between stator and rotor windings is embodied in the Thevenin voltage source as shown in (3.35) and (3.40), which can be calculated from the appropriate current values.

Based on (3.1), (3.3) and (3.30), (3.34) can be re-written as

$$\begin{bmatrix} \mathbf{Z}_{ss} & \mathbf{Z}_{sr} \\ \mathbf{Z}_{rs} & \mathbf{Z}_{rr} \end{bmatrix} = \mathbf{R} + \mathbf{Ars} + \frac{\mathbf{Lrs}}{\Delta t}$$

$$= \begin{bmatrix} \frac{L_m+L_s}{\Delta t}+r_s & 0 & \frac{L_m\cos\theta}{\Delta t}-\omega L_m\sin\theta & \frac{L_m\sin\theta}{\Delta t}+\omega L_m\cos\theta \\ 0 & \frac{N^2L_m+L_s}{\Delta t}+r_s & \frac{-NL_m\sin\theta}{\Delta t}-\omega NL_m\cos\theta & \frac{NL_m\cos\theta}{\Delta t}-\omega NL_m\sin\theta \\ \frac{L_m\cos\theta}{\Delta t}-\omega L_m\sin\theta & \frac{-NL_m\sin\theta}{\Delta t}-\omega NL_m\cos\theta & \frac{L_m+L_r}{\Delta t}+r_{cage} & 0 \\ \frac{L_m\sin\theta}{\Delta t}+\omega L_m\cos\theta & \frac{NL_m\cos\theta}{\Delta t}-\omega NL_m\sin\theta & 0 & \frac{L_m+L_r}{\Delta t}+r_{cage} \end{bmatrix}$$

$$(3.41)$$

in which

$$\mathbf{Z}_{ss} = \begin{bmatrix} \frac{L_m+L_s}{\Delta t}+r_s & 0 \\ 0 & \frac{N^2L_m+L_s}{\Delta t}+r_s \end{bmatrix} \tag{3.42}$$

$$\mathbf{Z}_{sr} = \begin{bmatrix} \frac{L_m\cos\theta}{\Delta t}-\omega L_m\sin\theta & \frac{L_m\sin\theta}{\Delta t}+\omega L_m\cos\theta \\ \frac{-NL_m\sin\theta}{\Delta t}-\omega NL_m\cos\theta & \frac{NL_m\cos\theta}{\Delta t}-\omega NL_m\sin\theta \end{bmatrix} \tag{3.43}$$

$$\mathbf{Z}_{rs} = \mathbf{Z}_{sr}^{\mathbf{T}} \tag{3.44}$$

$$\mathbf{Z}_{rr} = \begin{bmatrix} \frac{L_m+L_s}{\Delta t}+r_{cage} & 0 \\ 0 & \frac{L_m+L_s}{\Delta t}+r_{cage} \end{bmatrix} \tag{3.45}$$

19

$$\mathbf{Z_{th}} = \begin{bmatrix} Z_{aa} & Z_{ab} \\ Z_{ba} & Z_{bb} \end{bmatrix} = \mathbf{Z_{ss}} - \mathbf{Z_{sr}}\mathbf{Z_{rr}^{-1}}\mathbf{Z_{rs}} = \mathbf{Z_{ss}} - \mathbf{Z_{sr}} \left(\frac{L_m + L_s}{\Delta t} + r_{cage} \right)^{-1} \begin{bmatrix} 1 & 0 \\ 0 & 1 \end{bmatrix} \mathbf{Z_{sr}^T}$$

$$= \mathbf{Z_{ss}} - \frac{\Delta t}{L_m + L_s + r_{cage}\Delta t} \mathbf{Z_{sr}}\mathbf{Z_{sr}^T}$$

(3.46)

Now the calculation of $\mathbf{Z_{sr}}\mathbf{Z_{sr}^T}$ is considered. According to basic theory of matrix operations, $\mathbf{Z_{sr}}\mathbf{Z_{sr}^T}$ is a symmetrical 2 x 2 matrix [18]. The following deduction is to further verify the presumption that $\mathbf{Z_{sr}}\mathbf{Z_{sr}^T}$ is a diagonal matrix. Once $\mathbf{Z_{sr}}\mathbf{Z_{sr}^T}$ is proven to be diagonal, $\mathbf{Z_{th}}$ will also be a diagonal matrix since matrix $\mathbf{Z_{ss}}$ is diagonal.

$$\mathbf{Z_{sr}}\mathbf{Z_{sr}^T} = \begin{bmatrix} \dfrac{L_m\cos\theta}{\Delta t} - \omega L_m\sin\theta & \dfrac{L_m\sin\theta}{\Delta t} + \omega L_m\cos\theta \\[3mm] \dfrac{-NL_m\sin\theta}{\Delta t} - \omega NL_m\cos\theta & \dfrac{NL_m\cos\theta}{\Delta t} - \omega NL_m\sin\theta \end{bmatrix} \begin{bmatrix} \dfrac{L_m\cos\theta}{\Delta t} - \omega L_m\sin\theta & \dfrac{-NL_m\sin\theta}{\Delta t} - \omega NL_m\cos\theta \\[3mm] \dfrac{L_m\sin\theta}{\Delta t} + \omega L_m\cos\theta & \dfrac{NL_m\cos\theta}{\Delta t} - \omega NL_m\sin\theta \end{bmatrix}$$

$$= \begin{bmatrix} A & B \\ B & C \end{bmatrix}$$

(3.47)

$$A = \left(\frac{L_m\cos\theta}{\Delta t} - \omega L_m\sin\theta \right)^2 + \left(\frac{L_m\sin\theta}{\Delta t} + \omega L_m\cos\theta \right)^2 > 0 \qquad (3.48)$$

$$B = \left(\frac{L_m\cos\theta}{\Delta t} - \omega L_m\sin\theta \right)\left(\frac{-NL_m\sin\theta}{\Delta t} - \omega NL_m\cos\theta \right)$$
$$+ \left(\frac{L_m\sin\theta}{\Delta t} + \omega L_m\cos\theta \right)\left(\frac{NL_m\cos\theta}{\Delta t} - \omega NL_m\sin\theta \right)$$
$$= -N\left(\frac{L_m\cos\theta}{\Delta t} - \omega L_m\sin\theta \right)\left(\frac{L_m\sin\theta}{\Delta t} + \omega L_m\cos\theta \right) \qquad (3.49)$$
$$+ N\left(\frac{L_m\sin\theta}{\Delta t} + \omega L_m\cos\theta \right)\left(\frac{L_m\cos\theta}{\Delta t} - \omega L_m\sin\theta \right)$$
$$= 0$$

$$C = \left(\frac{-NL_m \sin\theta}{\Delta t} - \omega NL_m \cos\theta \right)^2 + \left(\frac{NL_m \cos\theta}{\Delta t} - \omega NL_m \sin\theta \right)^2 > 0 \quad (3.50)$$

The above derivation demonstrates that $\mathbf{Z_{th}}$ is a diagonal matrix.

$$\mathbf{Z_{th}} = \begin{bmatrix} Z_{aa} & 0 \\ 0 & Z_{bb} \end{bmatrix} \quad (3.51)$$

Reasonable selection of motor parameters can ensure that Z_{aa} and Z_{bb} are positive numbers. Based on (3.38) and (3.51), the branch currents of the two stator windings can be obtained as

$$I_{as}(t) = \frac{V_{as} - E_{thas}(t - \Delta t)}{Z_{aa}} \quad (3.52)$$

$$I_{bs}(t) = \frac{V_{bs} - E_{thbs}(t - \Delta t)}{Z_{bb}} \quad (3.53)$$

From (3.52), the stator main winding can be represented as a Norton equivalent branch with a shunt impedance of Z_{aa} and a history current source of $I_a(t - \Delta t)$. The $I_a(t - \Delta t)$ is defined as

$$I_a(t - \Delta t) = \frac{-E_{thas}(t - \Delta t)}{Z_{aa}} \quad (3.54)$$

In addition, V_{as} in (3.52) is the voltage across the Norton branch calculated by the network solution. The same approach can also be used to represent the stator auxiliary winding with (3.53). The equivalent circuit of the compressor motor implemented in the electro-magnetic transients analysis tool consists of two Norton equivalent branches connected in parallel.

21

3.4   Equivalent circuit

The original construction of the compressor single phase induction motor is again shown in Figure 3.4. The equivalent circuit connection implemented in PSCAD is given in Figure 3.5.
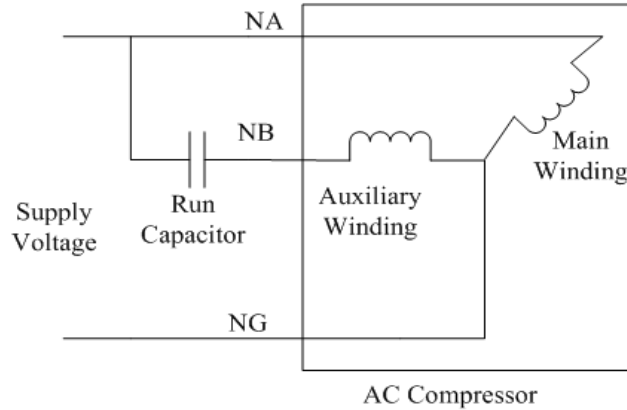

Figure 3.4 Original construction of air-conditioner compressor motor
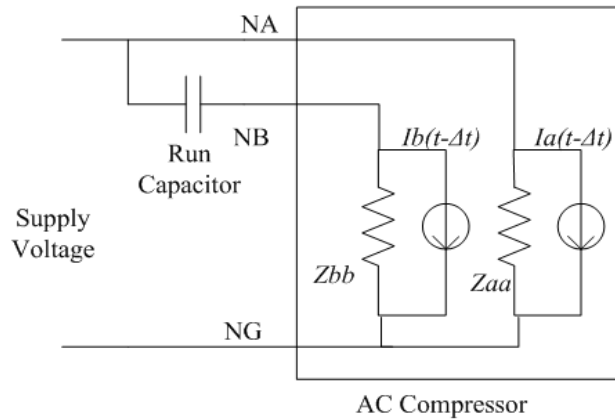

Figure 3.5 Equivalent schematic of compressor motor in PSCAD

The shunt admittances and history current sources of the two Norton branches are time-varying. Algebraic operations have been generated to calculate

the four variables associated with the equivalent circuit at every time step. The updated branch currents $I_{as}(t)$ and $I_{bs}(t)$ are also computed using the latest stator terminal voltage from the network solution to refresh air gap flux linkage, torque, speed and angle.

3.5   Solution process in PSCAD/EMTDC

EMTDC (Electro-Magnetic Transients including Direct Current), a simulation tool for electro-magnetic transients solution, represents and solves differential equations for both electro-magnetic and electro-mechanical systems in time domain. PSCAD (Power System Computer Aided Design) serves as the graphical user interface (GUI) for EMTDC [19].   PSCAD facilitates the construction and simulation of electric or control networks by placing and connecting specific components on a canvas.

The EMTDC solution engine consists of two main parts: The system dynamics module, which includes the master dynamics subroutine (DSDYN), the output definition subroutine (DSOUT), and the initialization subroutine (BEGIN); and secondly, the electric network solution module [19]. An EMTDC simulation begins at a specified start time and finishes at a specified end time. Between these two time instants, the program performs the same sequential process iteratively, and at each iteration the time is incremented by a specified interval [19]. The core EMTDC solution process is illustrated in Figure 3.6. First, variables are initialized and stored in BEGIN. Dynamic functions are implemented in DSDYN for updating electrical quantities of each component scanned in sequence from the PSCAD canvas. Each component has its own source code for the initialization

23

subroutine and the dynamics subroutine. The initialization subroutine called within the BEGIN directive of the PSCAD Fortran segment is generally used to pass the parameters entered through the component setting window into the EMTDC simulation engine. The dynamics subroutine of each component is automatically inserted into the system DSDYN in proper order. EMTDC assembles the source codes of all components, formulates the system admittance matrix and solves for new node voltages or branch currents of the electric network.

The external source code used to define the air-conditioner compressor single phase induction motor consists of two major subroutines. SPIM_RTC is used for data initialization as stated above. SPIM_EXE is called within the DSDYN segment of component definition, and used to run mathematical operations, update electrical and mechanical quantities and determine the currents drawn from the network. The detailed script of the source code is provided in the Appendix. The entire solution procedure of the developed model is given in Figure 3.7.
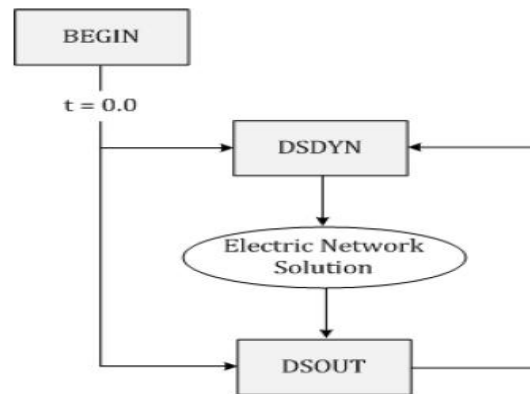

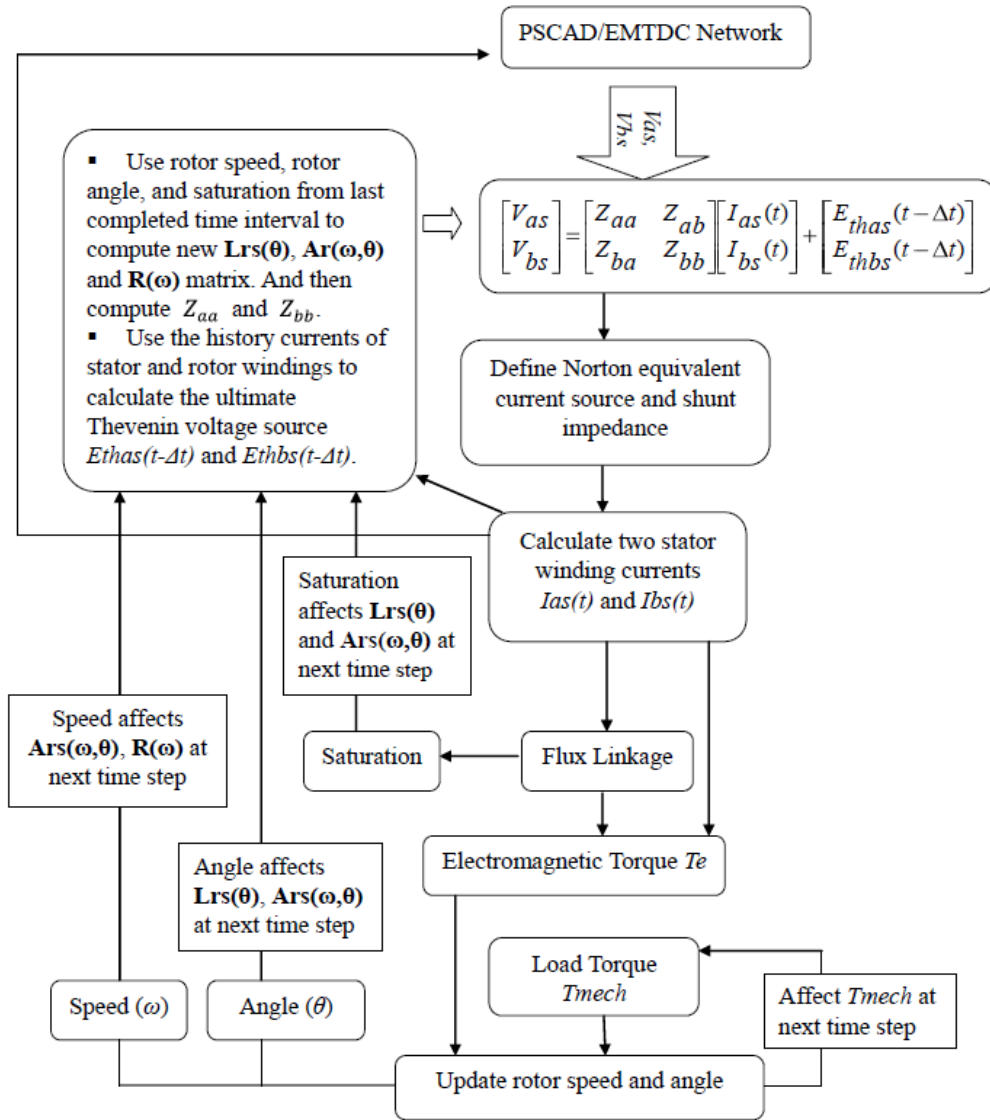Figure 3.6 Core EMTDC solution process [19]

24

Figure 3.7 Complete solution process of SPIM mode

Chapter 4.   SIMULATION OF INDIVIDUAL MOTOR

4.1   Simulation description

The behavior of the individual air-conditioner compressor is studied if a voltage depression occurs at different sinusoidal waveform points of the source voltage in this chapter. The test of a single unit of the custom motor model aims at validating the design of the model and selection of motor parameters. The individual custom model should have the same fidelity with the multiple motor units on a feeder. But it does not mirror the performance of the aggregate motors because of the delayed voltage recovery phenomenon on a feeder.

Each simulation is initialized by energizing the circuit for a while, allowing the motors to run up to speed against minimal load, applying the driven loads, and allowing conditions to stabilize before applying a voltage dip. The sequence of events is listed in Table 4.1

Table 4.1 Sequence of events

0.0 Sec.	Simulation starts, energize the circuit, apply speed-related loads.
0.5 Sec.	Apply angle-dependent driven loads
1.0 Sec. + Phase Delay	Apply programmed voltage dip
1.0 Sec. + Phase Delay + Fault Interval	Fault cleared, voltage recovers

4.2   Load torque

The mechanical load torque has been proposed to have a component proportional to the square of the speed, principally friction and windage load. Another component varying with the angular position of the crankshaft of the

26

driven reciprocating compressor is also considered. This load component has been

assumed to have a simple triangular wave form. The speed-related load is added

first and the angular position-related load is applied after a start-up interval. The

load profile is depicted in Figure 4.1.
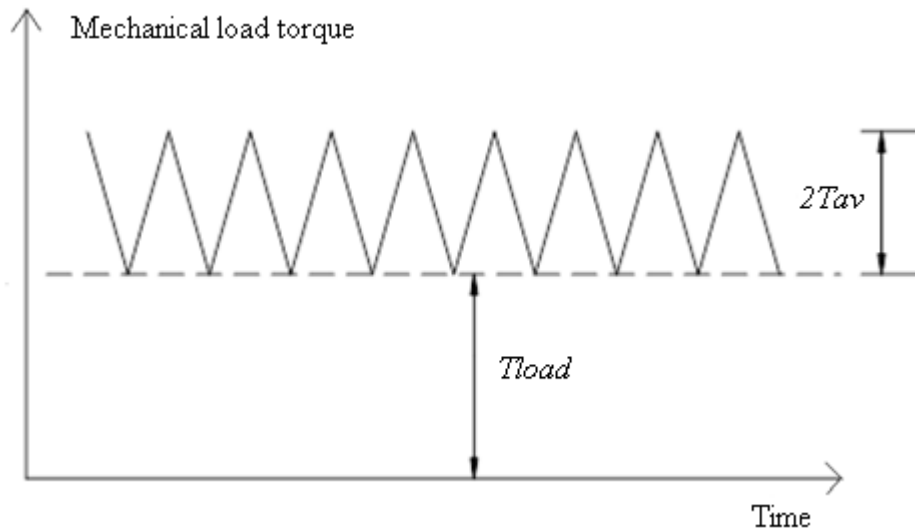
Figure 4.1. Steady state load torque [9]

In Figure 4.1, *Tload* represents the load torque component proportional to

the square of the speed. In steady state, *Tload* is almost constant because the

variation of speed is small. The load torque component related to the angular

displacement is varying triangularly with respect to simulation time with peak-to-

valley amplitude of two times *Tav*.

4.3 Distribution test system configuration

The distribution test system consists of a controllable voltage source, a

typical distribution transformer and a single unit of the custom motor. The motor

model is connected to the voltage source through the distribution transformer and

a lateral. The voltage source provides a supply voltage of 7.967 kV. After the

voltage drop across the lateral, the voltage is then lowered to 230 V by the distribution transformer to drive the custom motor model. The distribution transformer is rated at 7 kVA. The lateral has a pure inductance of 7 mH. The connection is shown in Figure 4.2. The block of motor model named "spim" in Figure 4.2 is represented by the equivalent circuit in Figure 3.5 in PSCAD.

Figure 4.2 Connection of individual motor test

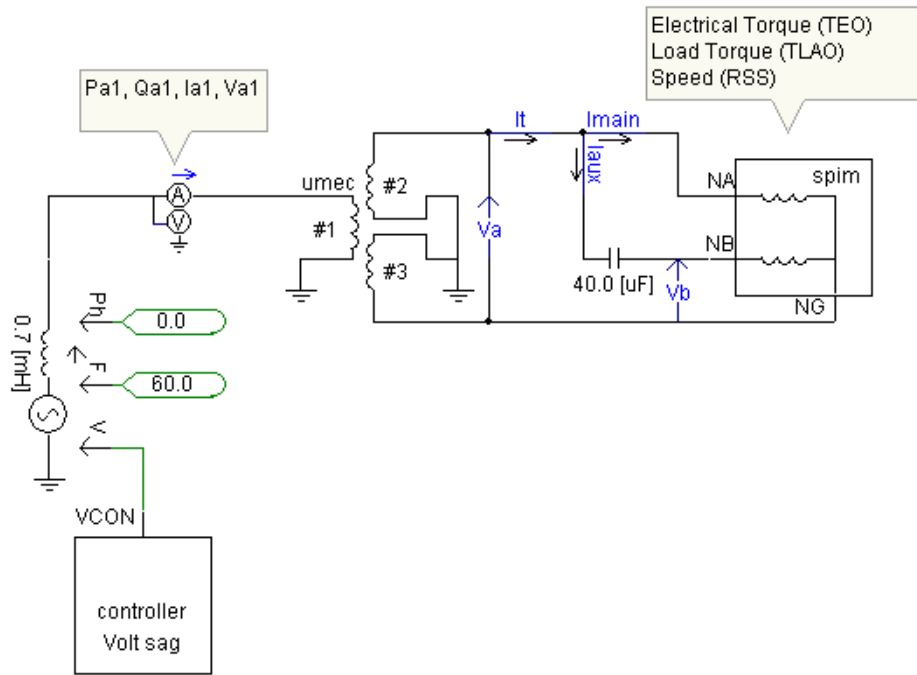A custom unit of the motor model represents tens of or hundreds of prototype motors determined by the scale factor entered through the parameter category window. Each prototype motor is loaded at 4.5 kW – 6.0 kW in various simulation cases. The rating of each prototype motor is determined by the average load torque applied to it.

The prototype motor parameters are given in Table 4.2.

Table 4.2 Parameters of each prototype motor

Scaling Factor	$scale=(1\text{-}177)$
Friction and Windage Load Coefficient (N-m)	$Tload = $ (typically 4, 6, or 8)$* scale$
Compressor Triangular Waveform Load Coefficient (N-m)	$Tav =$(typically 12, 8, or 4)$*scale$
Angular frequency (rad/s)	$\omega_o=377$
Stator winding resistance (ohms)	$rs=0.3/scale$
Rotor winding resistance at synchronous speed (ohms)	$rr=0.3/scale$
Unsaturated winding A to rotor mutual inductance (Henrys)	$L_{mu}=(30/\omega_o)/scale$
Winding A leakage inductance (Henrys)	$L_s=(0.5/\omega_o)/scale$
Rotor winding leakage inductance (Henrys)	$L_r=(0.2/\omega_o)/scale$
Turns ratio of winding bs to winding as (Henrys)	$N=1.4$
Auxiliary winding capacitor (Farads)	$ccap=(40e\text{-}6)*scale$
Rotor shaft length (m)	$length=0.2$
Rotor shaft diameter (m)	$diam=0.065$
Moment of inertia (kg*m^2)	$H_r=7800*(pi/32)*length*diam\text{^}4*scale$

The rating of each prototype motor is computed by

$$S_1 = (Tload + Tav)\omega_o \qquad\qquad (4.1)$$

The total MVA rating of a custom unit of the motor model representing a group of prototype motors is

$$S_{total} = S_1 * scale \qquad\qquad (4.2)$$

Different levels of air-conditioner loading of each prototype motor for simulation are tabulated in Table 4.3.

Table 4.3. Air-conditioner loading of each prototype motor

Nominal Power (kW)	Speed-Dependent Torque *Tload* (N-m)	Triangular Torque *Tav* (N-m)	Average Torque (N-m)
4.52	8	4	12
5.28	6	8	14
6.03	4	12	16

4.4 Simulation results and analysis

Two groups of studies are investigated in this chapter. As discussed above, the "prone-to-stall" motors are sensitive to voltage depression and specific points on voltage waveform at which the fault is applied. The first simulation scenario deals with dynamic responses of individual unit of motor model to different voltage dip levels when the fault occurs at the zero-crossing point of voltage waveform at the primary side of the distribution transformer. The second simulation scenario investigates the performance of the motor under different mechanical loadings when the fault is applied at 0, 45 and 90 degrees separately on the voltage waveform. The electrical quantities that have been monitored are included in Figure 4.3.
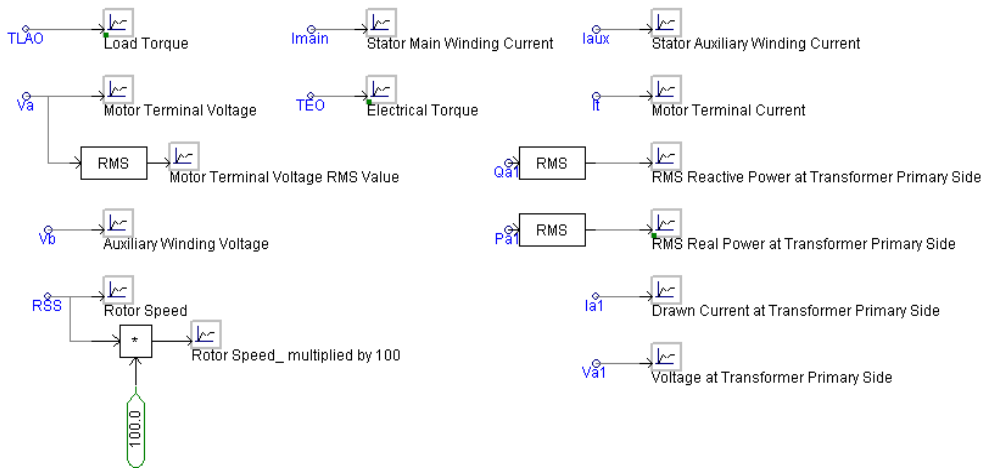

Figure 4.3 Electrical quantities monitored for individual motor test

30

The motor speed during the start-up process is plotted in Figure 4.4. The motor is prompted to start running and stabilize at rated speed by supply source in around 0.25 sec. Rapid change of voltage is considered to study the fast transient behavior of the motor model. The sensitivity of voltage source is maintained by setting a small input time constant for it so that the voltage source can sense the voltage change programmed by user and make adjustment quickly. As a compromise, the start-up transient of motor is obvious, which is reflected in the large speed variation, high start-up current, and bulky active and reactive power absorbed during that interval. A two-cylinder air-conditioner single phase induction motor is modeled in this thesis. Speed ripples of double fundamental frequency (120 Hz) appear on the speed plot.
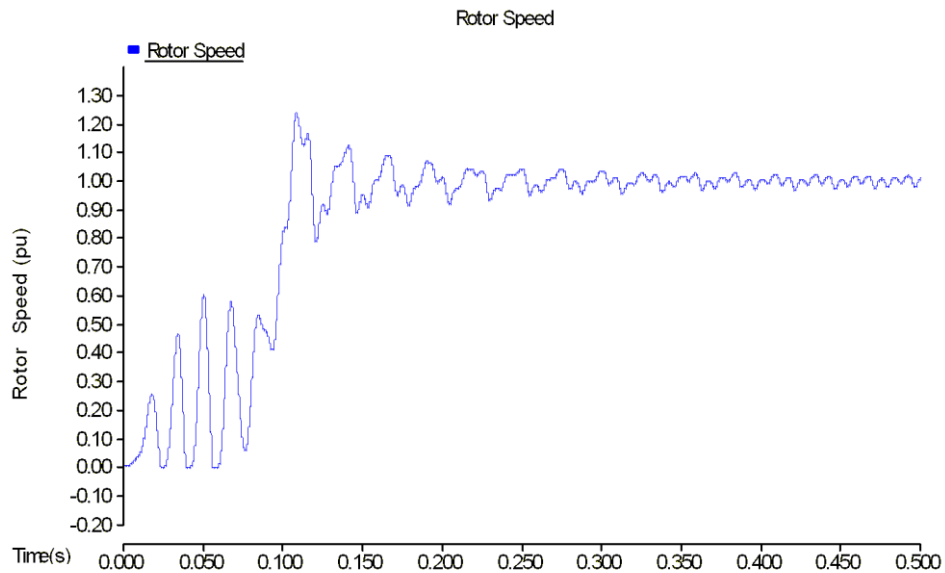

Figure 4.4 Start-up transients of motor model

31

4.4.1   Impacts of voltage depression

In this case, the impacts of no voltage depression, voltage depression to 80% of rating and to 60% of rating at the motor terminal are investigated. The voltage dip occurs at the 0 degree point of its sinusoidal wave, which occurs at 1 second in the simulation time domain. The applied voltage depression lasts for 5 cycles. The parameters of each prototype motor are given in Table 4.2 with a scale factor of 1. The average load torque applied to the unit is 14 N-m, consisting of 6 N-m speed-dependent torque (*Tload*) and 8 N-m triangular torque (*Tav*). The simulation conditions are given in Table 4.4.

Terminal current drawn by the unit is plotted to demonstrate that the model captures the real-time behaviors of single phase motor accurately. Electrical torque, load torque and motor speed are plotted on the same figure for convenient comparison between cases. The plots of motor terminal currents simulated with three voltage dip levels are given in Figure 4.5, Figure 4.7 and Figure 4.10. Plots of electrical torque, load torque and motor speed are presented in Figure 4.6, Figure 4.8, Figure 4.9 and Figure 4.11.

Table 4.4 Simulation conditions of the study of voltage depression level

Average load torque	Point-on-wave	Voltage dip initiates at	Dip duration	Three voltage depression levels
14 N-m	0 degrees	1 s	5 cycles	No dip, dip to 80% and 60% of normal value
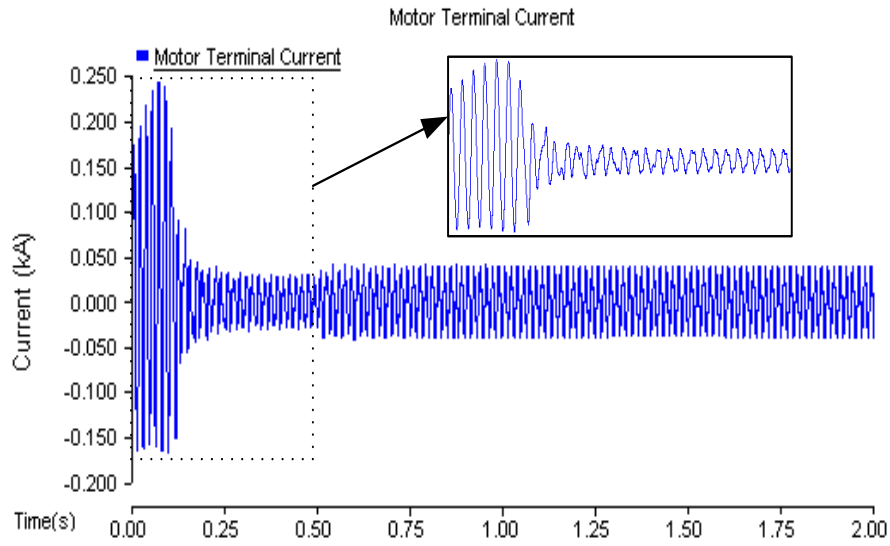
Figure 4.5 Motor terminal current (no voltage dip)
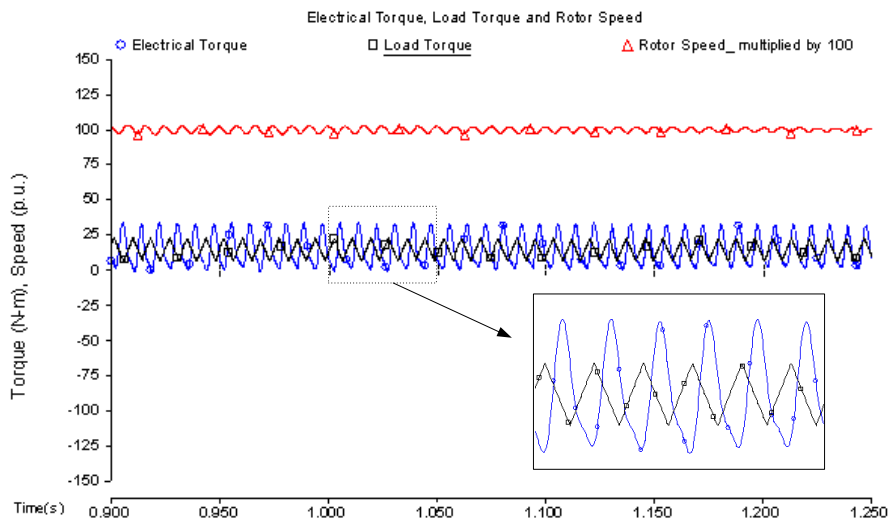
Figure 4.6 Electrical torque, load torque and scaled motor speed (no voltage dip)

Figure 4.7 Motor terminal current (voltage dips to 80% of normal value)
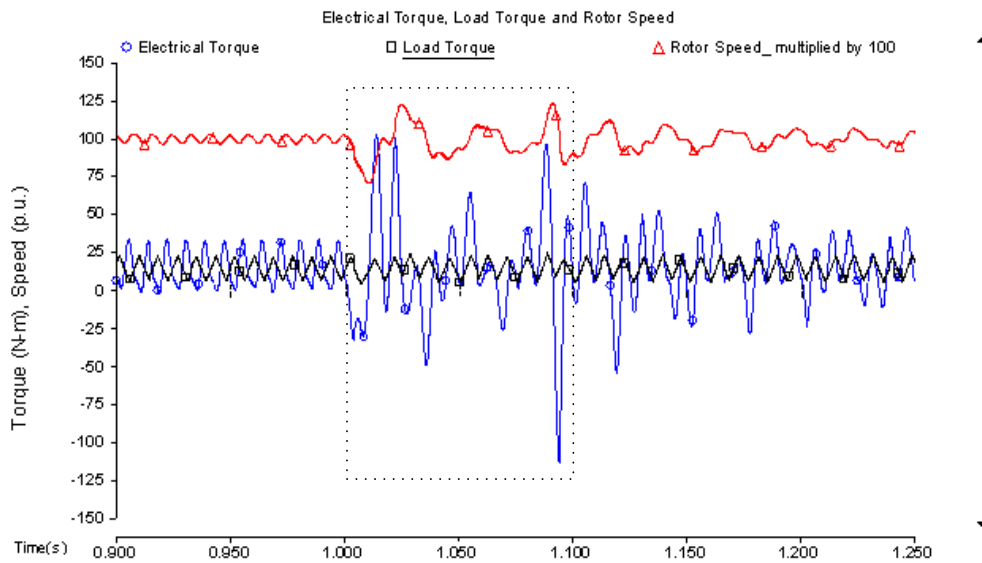
Figure 4.8 Electrical torque, load torque and scaled motor speed (voltage dips to 80% of normal value)
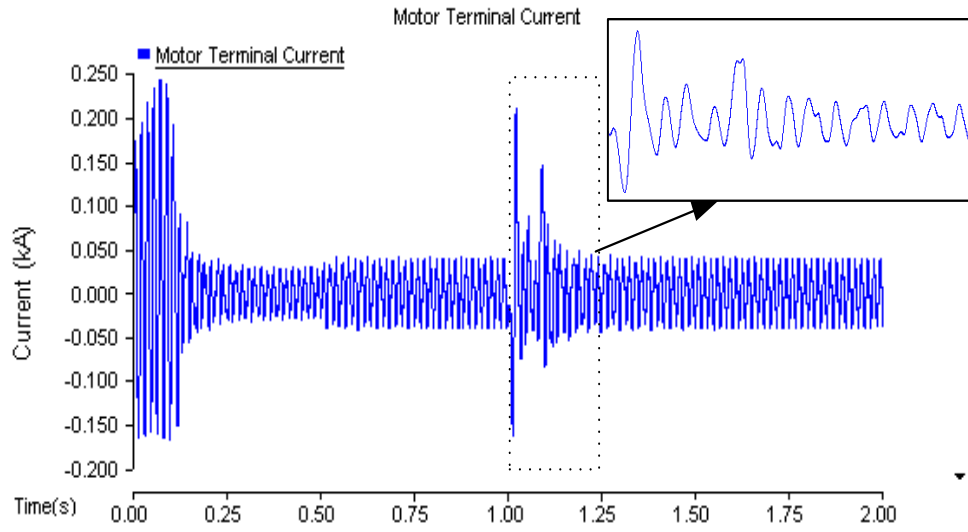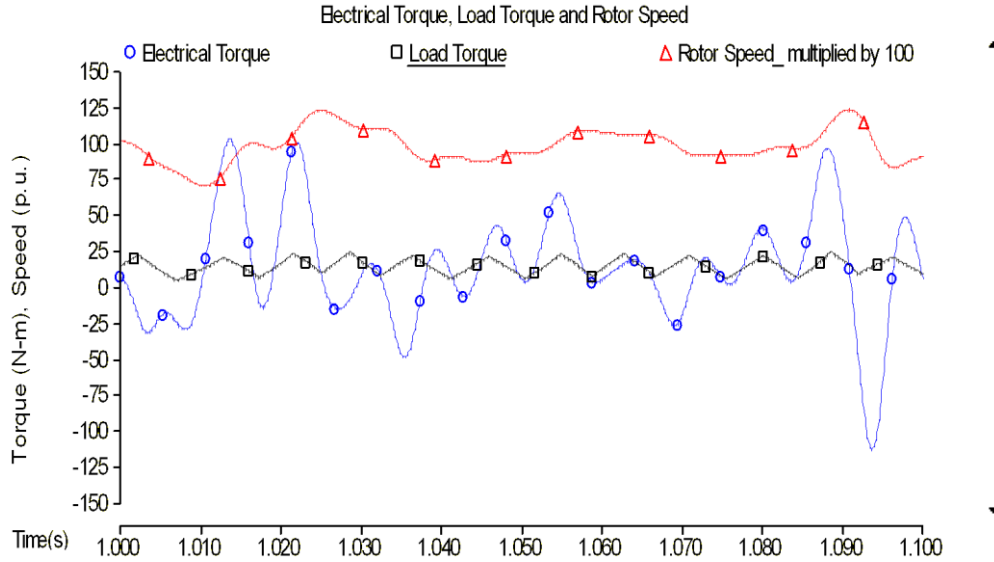
Figure 4.9 Zoomed in plot of electrical torque, load torque and scaled motor speed
(voltage dips to 80% of normal value)
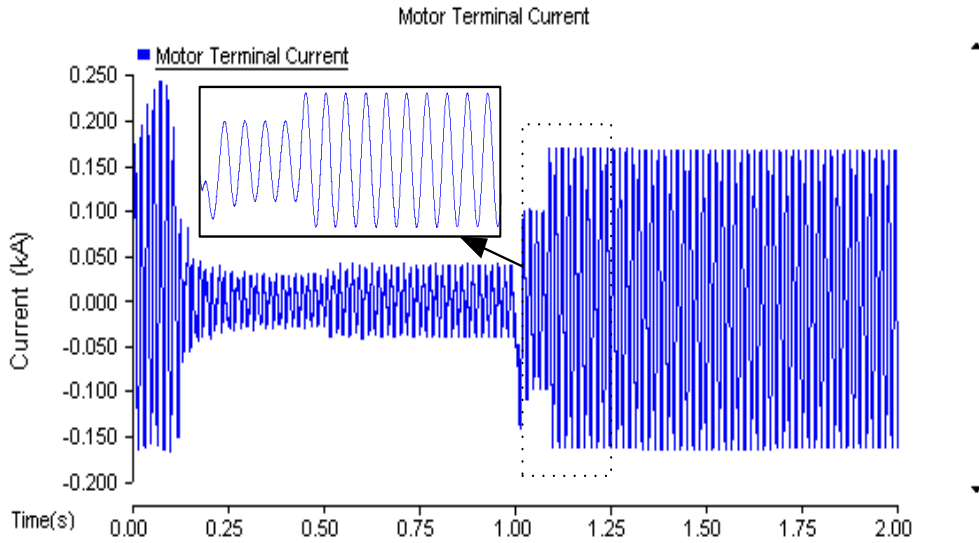
Figure 4.10 Motor terminal current (voltage dips to 60% of normal value)
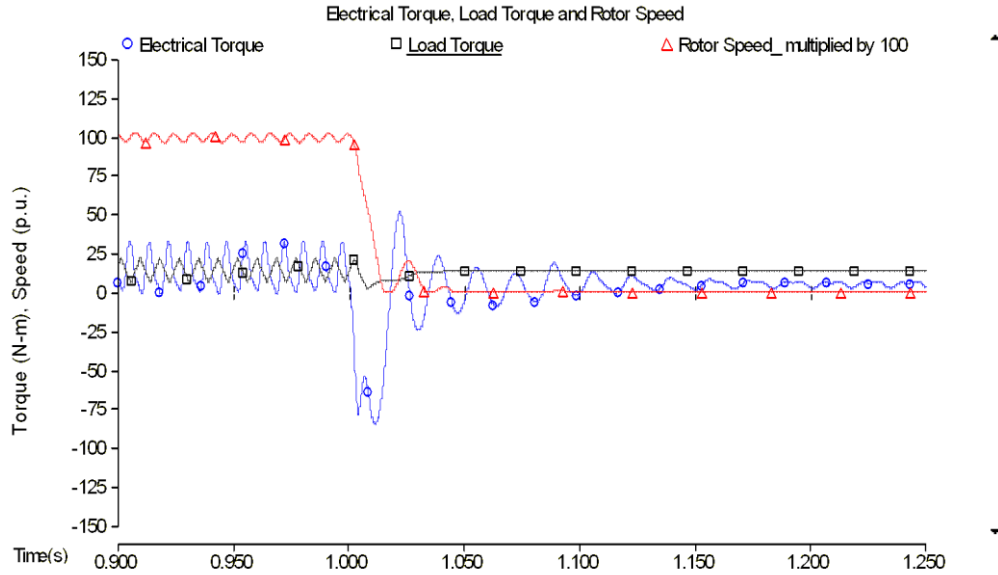
Figure 4.11 Electrical and load torque and scaled motor speed (voltage dips to 60% of normal value)

It is clearly observed from Figure 4.5 and Figure 4.7 that the start-up current and current during voltage dip transient are significantly high. The current curve depicted in Figure 4.10 indicates that stalled motor draws as large as five times of normal current.

From the simulations results in section 4.4.1, it is truthful to believe that air-conditioner compressor single phase induction motor is sensitive to sudden reduction in its terminal voltage. There is no unique quantitative answer to stalling voltage because the point where voltage dip is applied and dip duration also influence motor stalling. Large number of simulation cases need to be run with specific constraints to define an approximate and reasonable stalling voltage for consultation purpose in the future.

36

4.4.2   Point-on-wave (P-O-W) study

The motor is operating at three different mechanical loadings. Motors are prone to stall with heavier loads, especially when voltage dip occurs at zero degree point and less likely to stall with lighter loads when voltage drops at peak point of its waveform. The simulation profile is given in Table 4.5. Nine combinations of point-on-wave (P-O-W) and load torque have been formulated. Nine runs of simulation have been completed and the statistic data has been generalized in Table 4.6. From Table 4.6, it is concluded that the dip point on voltage wave will make a big difference in determining the running condition of the motor after voltage sag. Even heavily loaded motor (16 N-m average load torque) will not stop if the voltage depression is applied at peak point of its waveform. Electrical torque, load torque and speed plots of the 9 combinations of simulation are presented in Figure 4.12 through Figure 4.20.

Table 4.5 Simulation profile of P-O-W study

Average load torque (N-m)	12, 14 and 16
Point-on-wave(°)	0, 45 and 90
Time (s)	1.00, 1.0021 and 1.0042
Voltage dip duration (cycles)	5
Voltage depression level	Dip to 60% of normal value

Table 4.6 Statistic results of motor stalling of nine simulation runs

Point-on-wave (°)	*Tload* (N-m)	*Tav* (N-m)	Average load torque (N-m)	Stall or Not-stall
0	8	4	12	Not-stall
0	6	8	14	Stall
0	4	12	16	Stall
45	8	4	12	Not-stall
45	6	8	14	Not-stall
45	4	12	16	Stall
90	8	4	12	Not-stall
90	6	8	14	Not-stall
90	4	12	16	Not-stall

Figure 4.12 Plot of electrical and load torques and motor speed when load torque is 12 N-m and fault is applied at 0 degree of voltage waveform

38
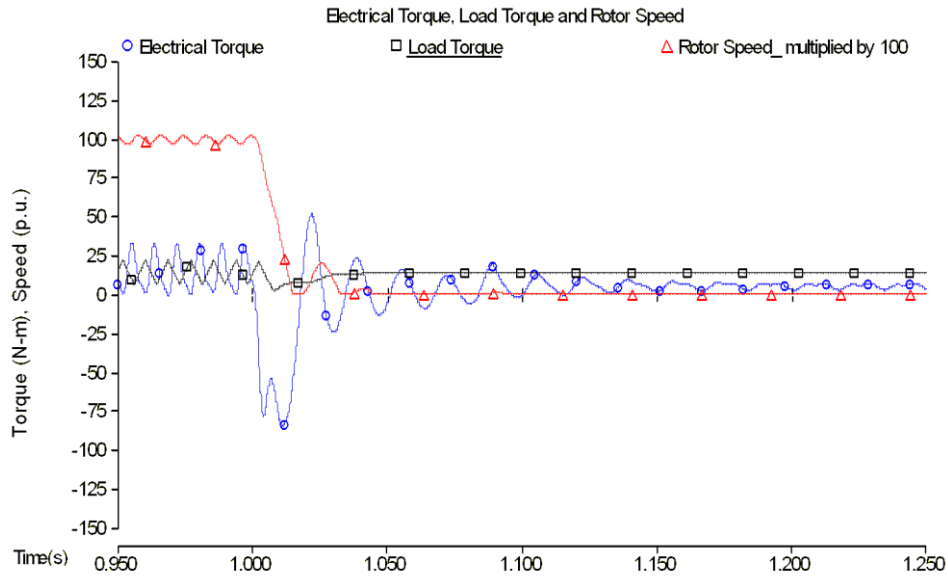
Figure 4.13 Plot of electrical and load torques and motor speed when load torque
is 14 N-m and fault is applied at 0 degree of voltage waveform
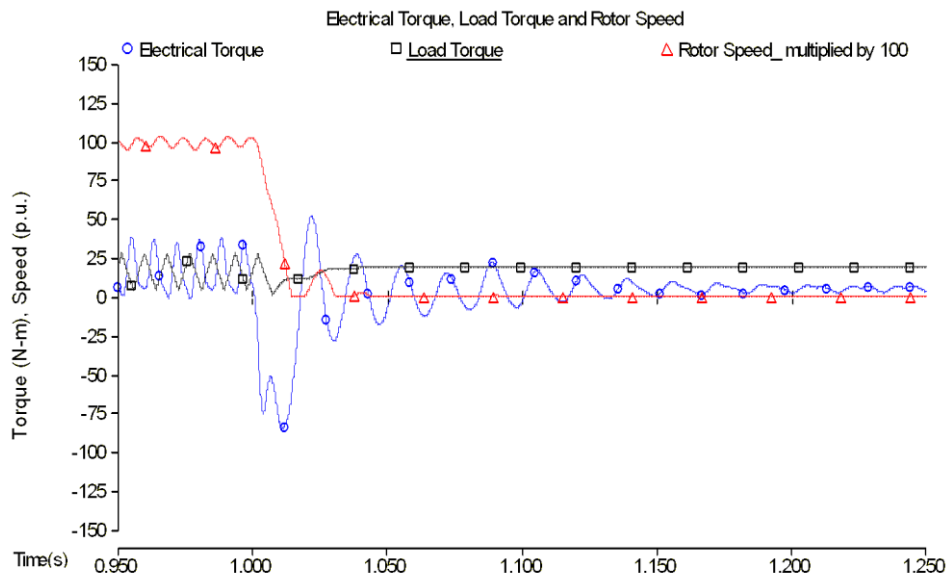
Figure 4.14 Plot of electrical and load torques and motor speed when load torque
is 16 N-m and fault is applied at 0 degree of voltage waveform
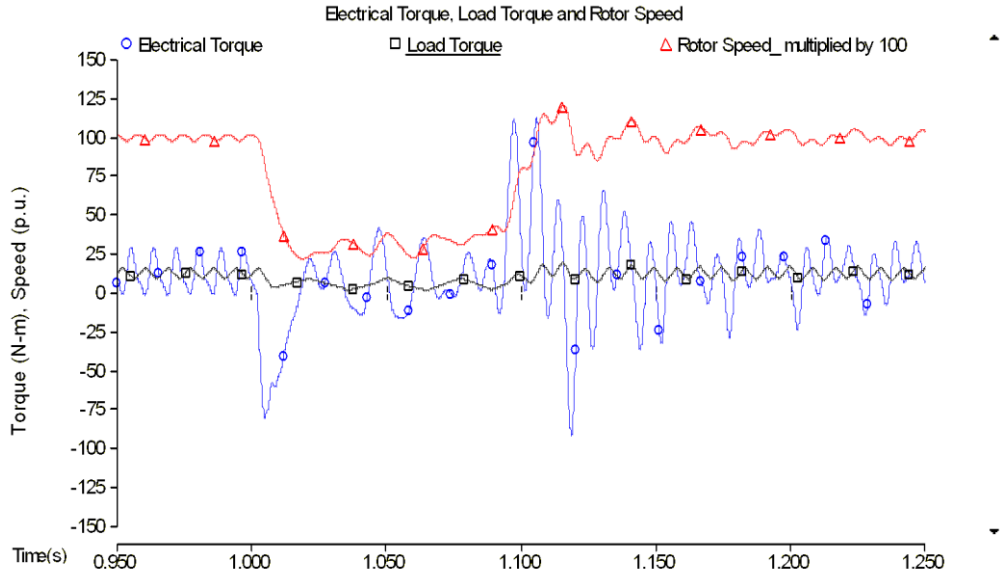
Figure 4.15 Plot of electrical and load torques and motor speed when load torque is 12 N-m and fault is applied at 45 degrees of voltage waveform
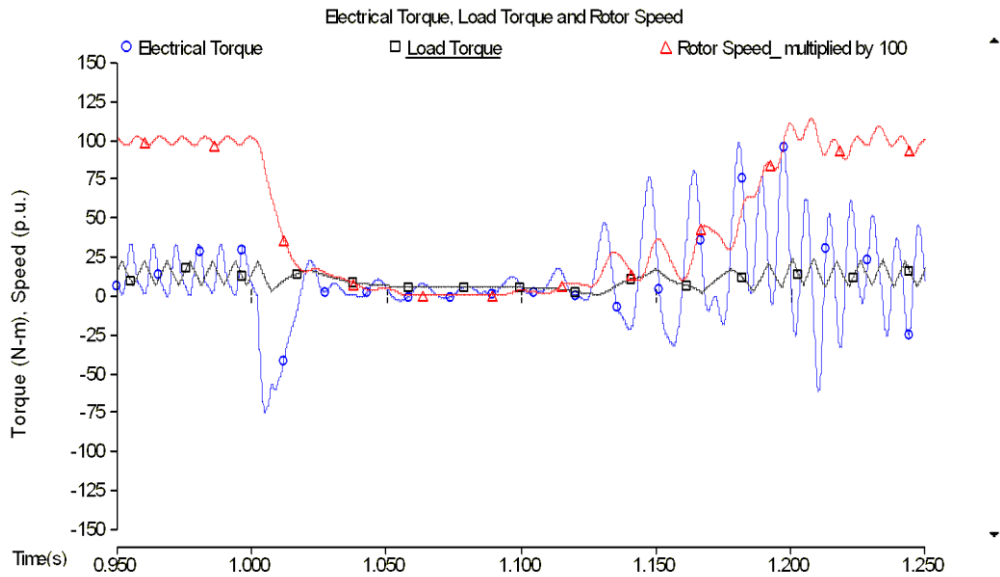
Figure 4.16 Plot of electrical and load torques and motor speed when load torque is 14 N-m and fault is applied at 45 degrees of voltage waveform

40
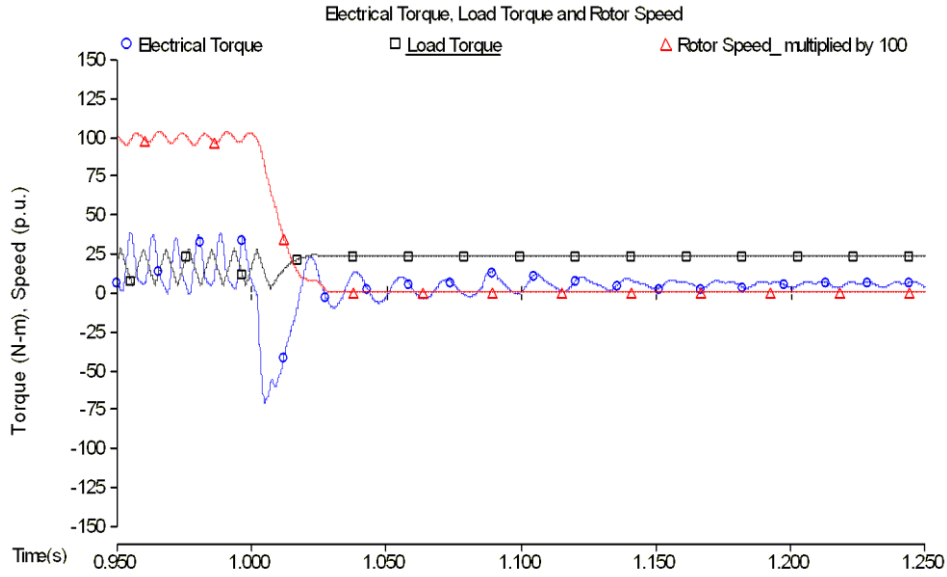
Figure 4.17 Plot of electrical and load torques and motor speed when load torque is 16 N-m and fault is applied at 45 degrees of voltage waveform
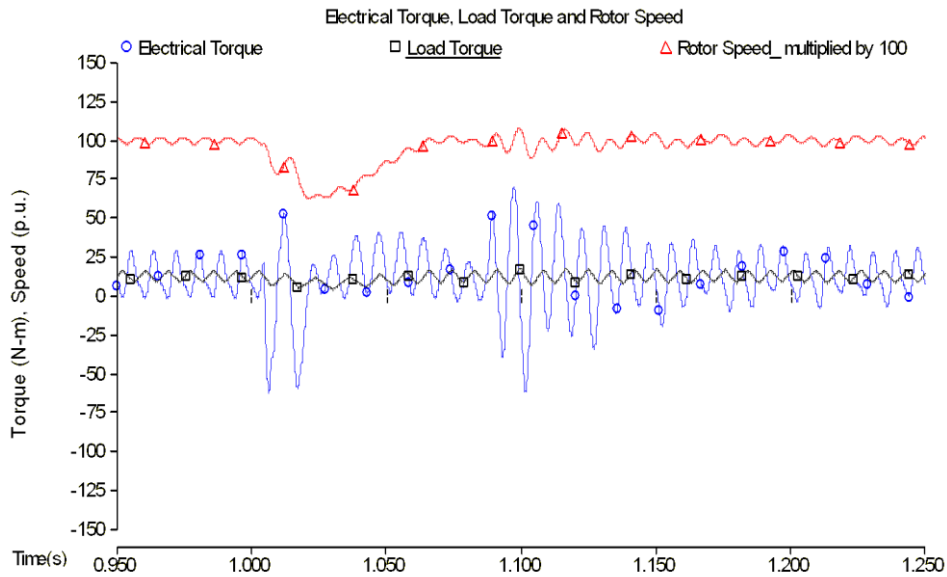
Figure 4.18 Plot of electrical and load torques and motor speed when load torque is 12 N-m and fault is applied at 90 degrees of voltage waveform
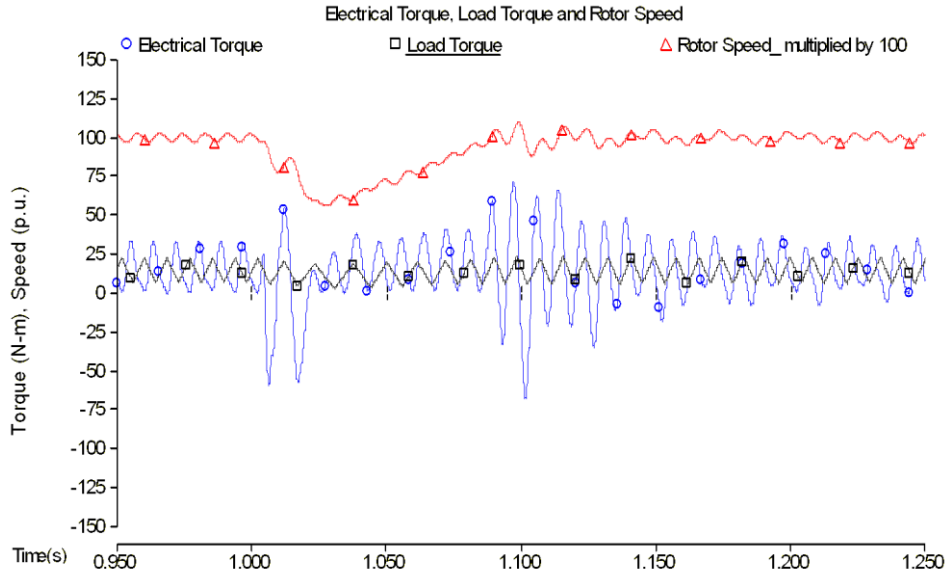
Figure 4.19 Plot of electrical and load torques and motor speed when load torque is 14 N-m and fault is applied at 90 degrees of voltage waveform
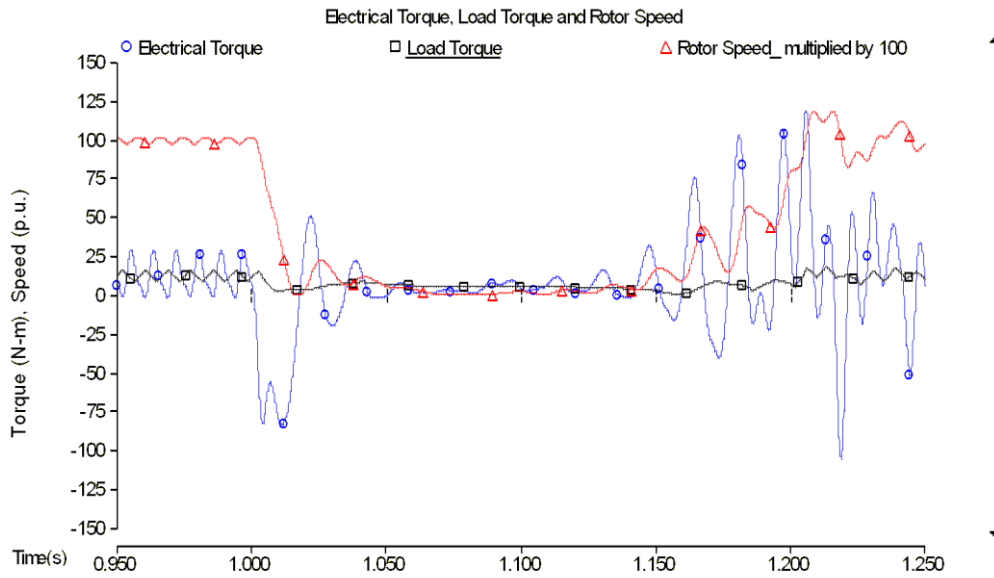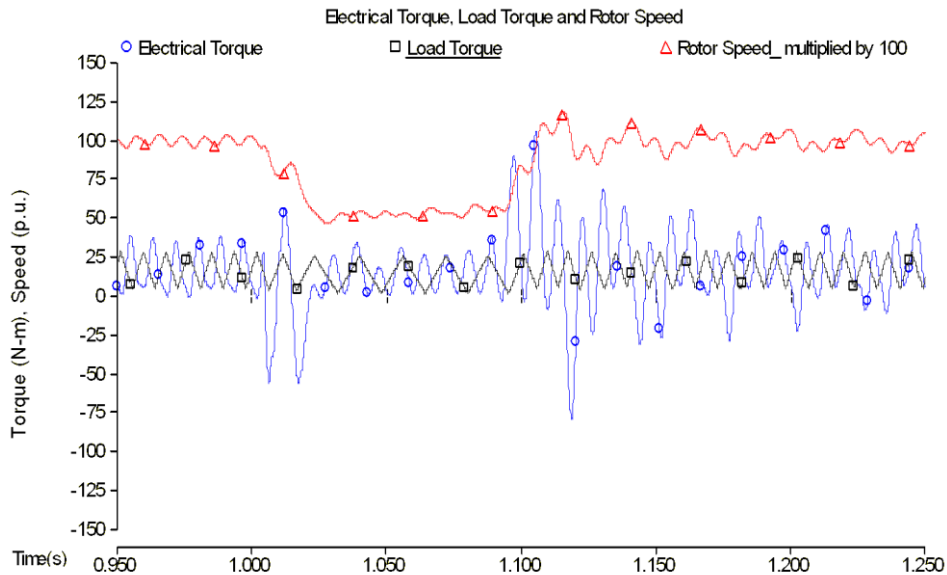

Figure 4.20 Plot of electrical and load torques and motor speed when load torque is 16 N-m and fault is applied at 90 degrees of voltage waveform

It is observed from Figure 4.12 through Figure 4.20 that whether a motor stalls or not depends on the encircled area between electrical torque and load

42

torque curves during the short interval immediately after the voltage dip is applied. The load torque is larger than electrical torque in this short period, which results in motor deceleration. According to (3.15), the speed change is proportional to the size of area determined by electrical and load torque curves. Clear comparisons between Figure 4.14 and 4.15, and Figure 4.17 and 4.18 are shown to justify the above statement. Another important phenomenon that can be found from Figure 4.12, Figure 4.15 and Figure 4.16 that the motor can reaccelerate from very low speed to normal value with large positive components of electrical torque after the fault is cleared. In general, the electrical torque induced by unidirectional currents is closely associated with motor stalling.

Chapter 5.   SIMULATION WITH MULTIPLE UNITS

5.1   Feeder model

The study in this chapter considers a realistic radial three-phase distribution feeder as shown in Figure 5.1. The entire feeder consists of 8 coupled PI-section blocks of the feeder line. The feeder is split into two branches at node 8. Seven concentrated load blocks are coupled with the feeder at seven different nodes. Each concentrated block of load consists of 0.2 MW constant lighting load and a bundle of 177 prototype motors where each motor is loaded at 5.28 kW. The parameters of each prototype motor are given in Table 4.2. The loading information is given in Table 4.3. The schematic of the distribution feeder constructed in PSCAD is given in Figure 5.2.

5.1.1   System configuration

The three-phase supply is modeled by three single phase sources with phase shift of 120 degrees so that asymmetrical voltage sag can be played in. Each of the single phase sources has a Thevenin inductance of 0.7 mH. The series link from node 1 to node 2 has an inductance of 3.5 mH for each individual phase. The main supply transformer is connected wye-wye with both neutral points solidly grounded. Each block of load is coupled to the feeder node through a typical distribution transformer. The single phase distribution transformers are connected phase-ground on the primary side. For the secondary side of the transformer, the custom motor model is connected in parallel with the secondary winding and the neutral point of this winding is grounded effectively. The

constant resistive lighting loads are divided into two equal parts and each part has

a phase-ground connection on the secondary side of the distribution transformer.

The specifications of the realistic feeder are given in Table 5.1.

Table 5.1 Specifications of realistic feeder

Supply transformer	
Primary winding voltage (L-L / L-N)	121.24 kV (L-L) / 70 kV (L-N)
Secondary winding voltage (L-L / L-N)	13.8 kV (L-L) / 7.967 kV (L-N)
MVA base	8 MVA
Impedance (on base MVA)	0.002+j0.08 per unit
PI-section feeder line	
Positive sequence series impedance	0.43+j0.43 ohms/mile
Zero sequence series impedance	1.70+j0.67 ohms/mile
Distribution transformer	
Primary side voltage	7967 V
Secondary side voltage	115 V/115 V center grounded
MVA base	1.5 MVA
Impedance (on base MVA)	j0.02 per unit

5.1.2   Contingency description

The feeder is set up with unbalanced loading. Phase-C serves three

concentrated loads while phases-A and -B serve two loads each. Phase-C is

heavily loaded and has a greater voltage drop than the other two phases from its

head to its tail. The voltages on the feeder and at the motor terminals are not

constant in the pre-event conditions. They vary slightly as the effect of angle

dependent component of load torque. A voltage depression event is generated to

dip the voltage on phase-A and phase-C from initial 70 kV (L-N) down to 41.2

kV. The voltage on phase-B is maintained unchanged. The simulation condition is

given in Table 5.2.

Table 5.2 Simulation condition of feeder with multiple units

A/C loading	$Tload$=6 N-m and Tav=8 N-m
Voltage at bottom of dip for both A and C phases	41.2 kV
Point-on-wave (on phase-C)	0 degrees
Time when voltage dip is applied	1.0111 sec
Dip duration	0.0833 sec
Simulation time step	20 us
Data points collected	every 16 points

The pre-event voltages at the head of the feeder which is node 3, at node 8 and at node 11 are recorded and given in Table 5.3.

Table 5.3 Pre-event voltages at three nodes

Phase	Node 3 (kV)	Node 8 (kV)	Node 11 (kV)
Van	7.76	7.62	7.50
Vbn	7.79	7.50	7.48
Vcn	7.66	7.00	6.84

Motor terminal voltages are also measured and shown in Table 5.4.

Table 5.4. Pre-event Voltages at Motor Terminals

Motor number	Phase	RMS / V
M1	A	216.41
M2	C	209.00
M3	B	212.36
M4	C	197.89
M5	B	208.56
M6	A	211.34
M7	C	192.60

5.1.3   Air-conditioner loading

The schematic of distribution feeder implemented in PSCAD is given in Figure 5.1. And the picture of a detailed unit of load block is presented in Figure 5.2.
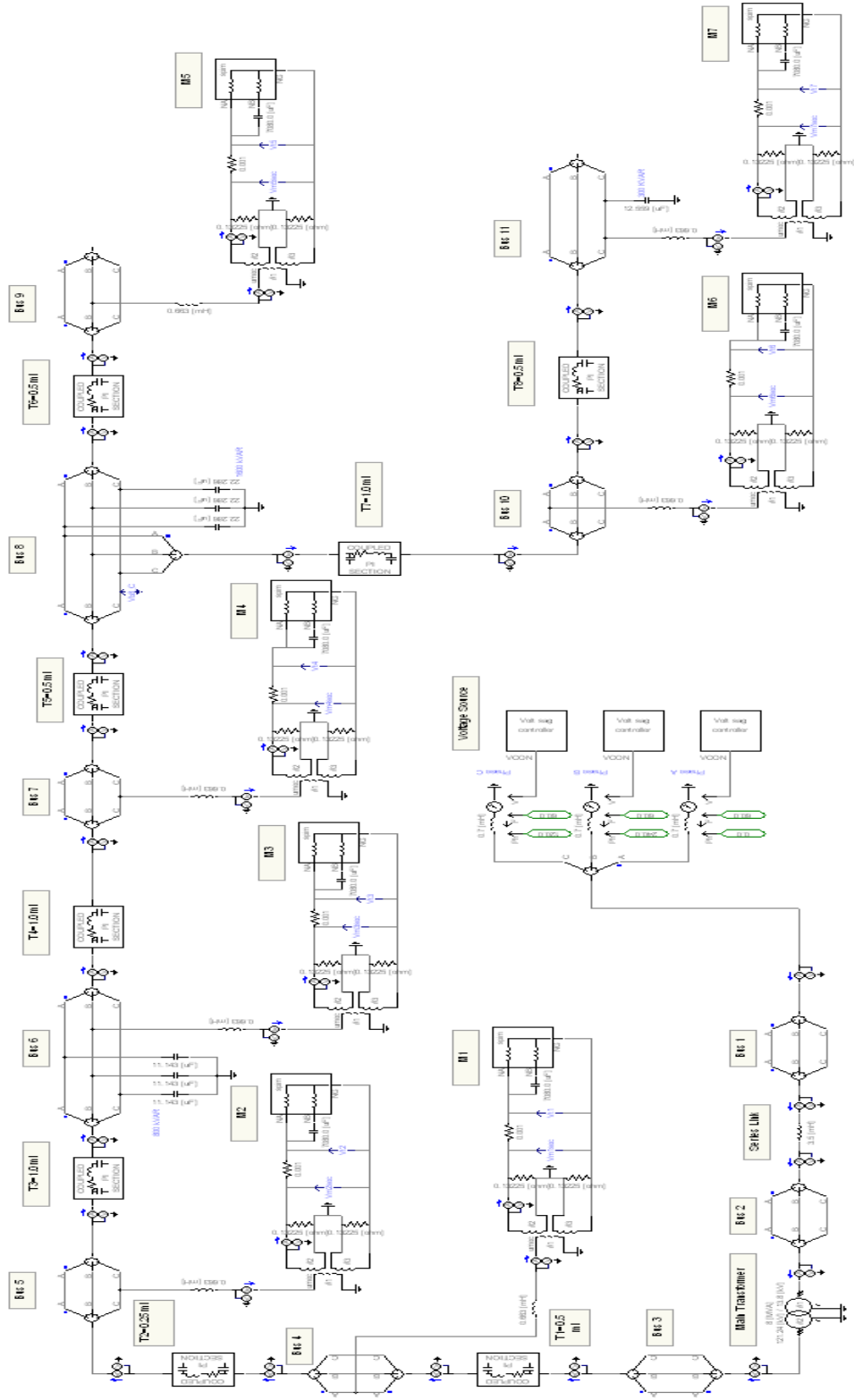
Figure 5.1 Realistic feeder implemented in PSCAD
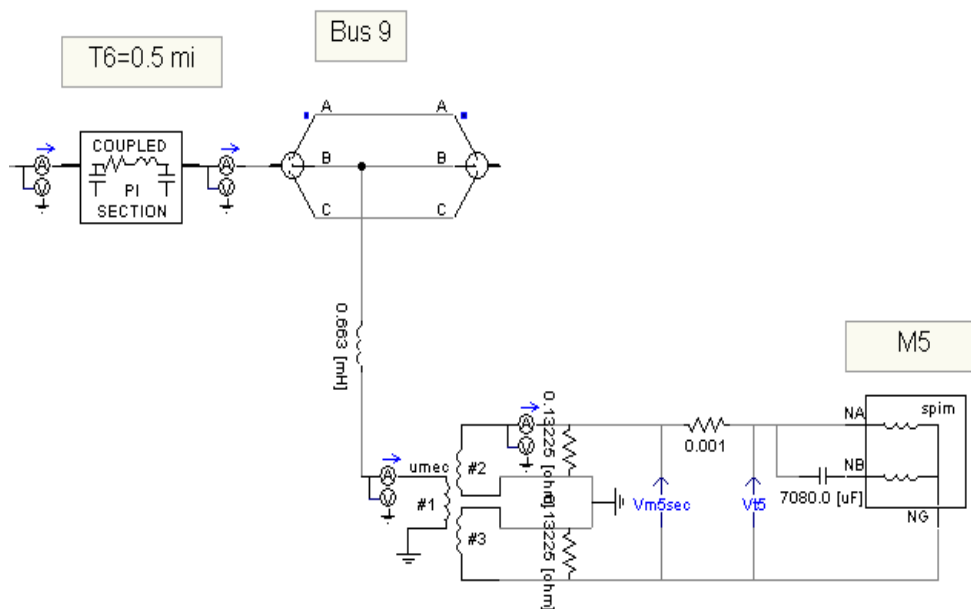
Figure 5.2 Connection of each block of load to the feeder through the distribution transformer

5.2 Simulation results

The terminal voltage of motor 7 is shown in Figure 5.3. The electrical torque, load torque and speed of each motor are plotted in Figure 5.4 through Figure 5.11 for analysis. The speed plots of all seven motors are shown in Figure 5.12. The three-phase currents at the primary side of main transformer are plotted in Figure 5.13.

48
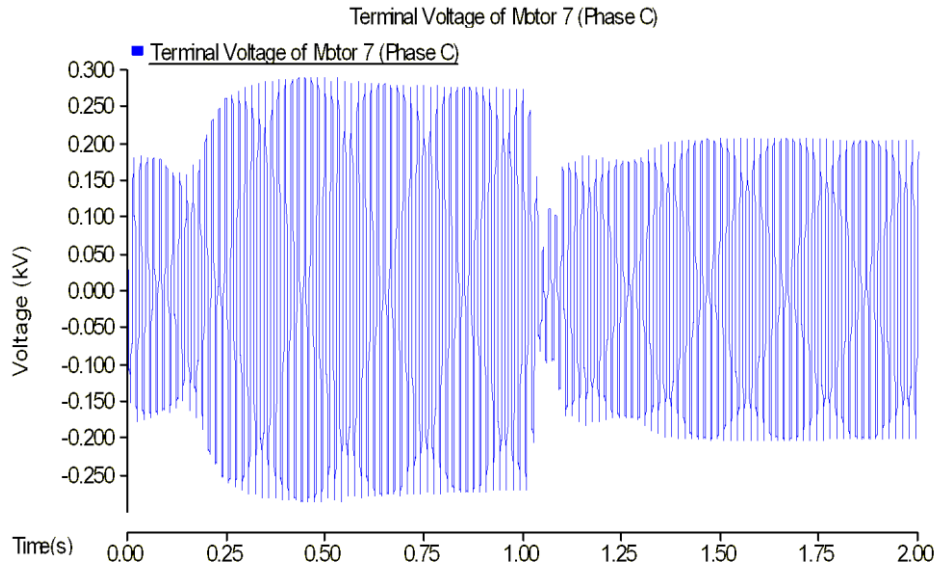
Figure 5.3 Terminal voltage of motor 7
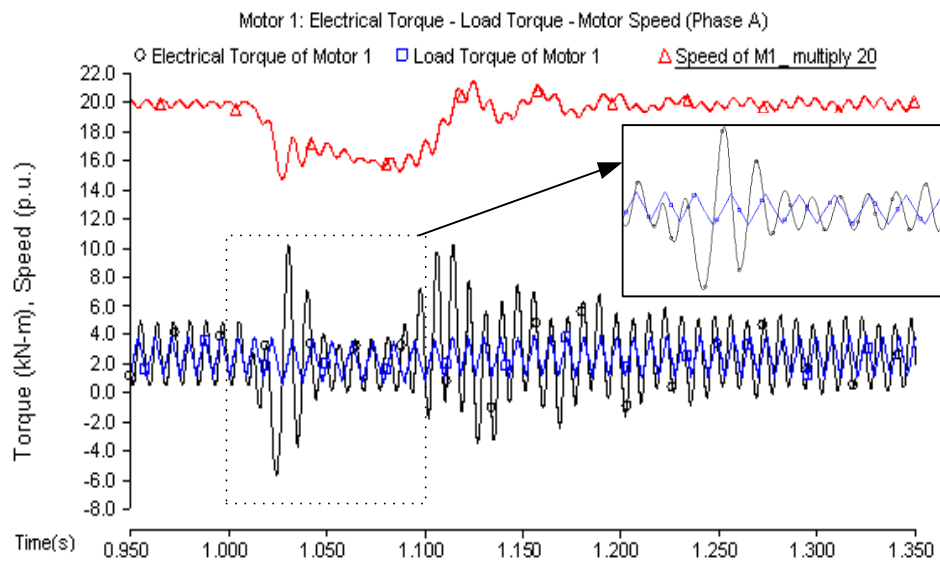
Figure 5.4 Plot of electrical torque and load torque, and scaled speed of motor 1 (Phase-A)
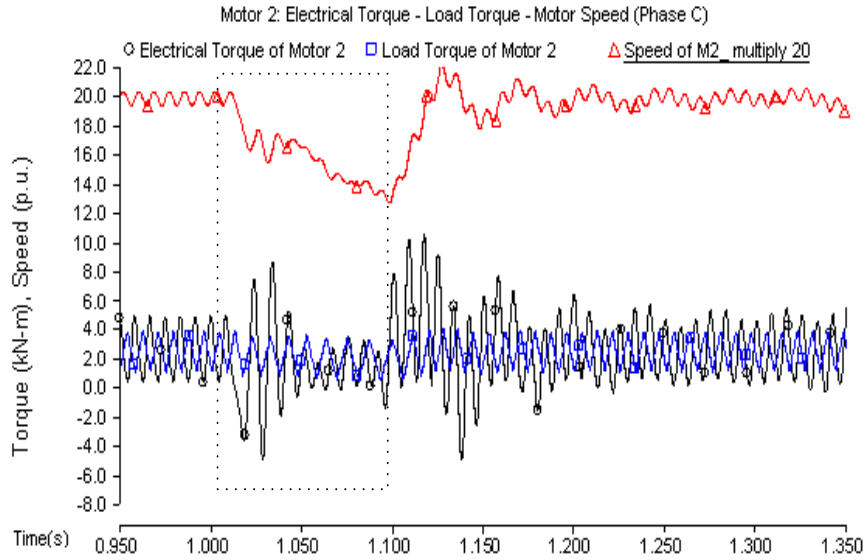
Figure 5.5 Plot of electrical torque and load torque, and scaled speed of motor 2 (Phase-C)
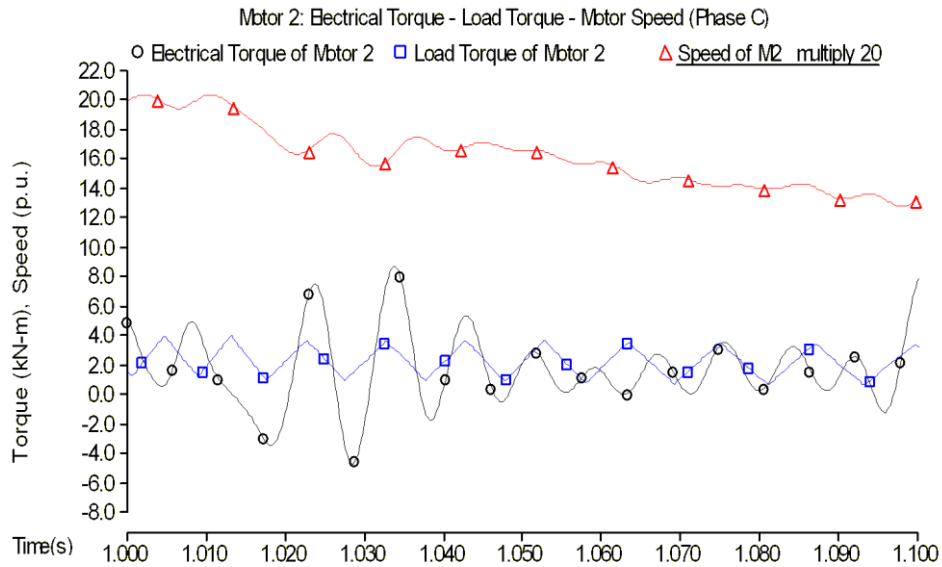
Figure 5.6 Zoomed in plot of electrical torque, load torque and scaled speed of motor 2 (Phase-C)
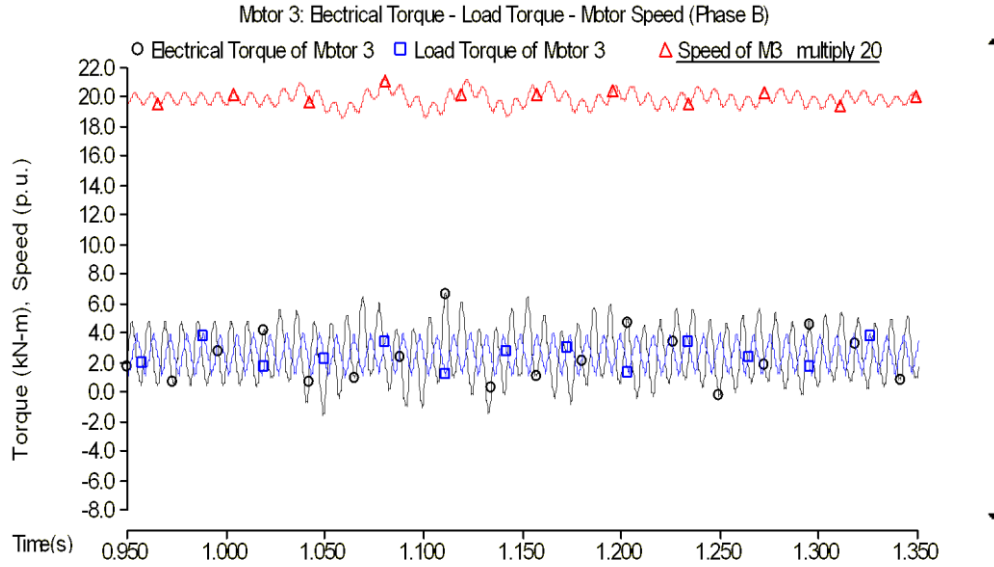
Figure 5.7 Plot of electrical torque and load torque, and scaled speed of motor 3 (Phase-B)
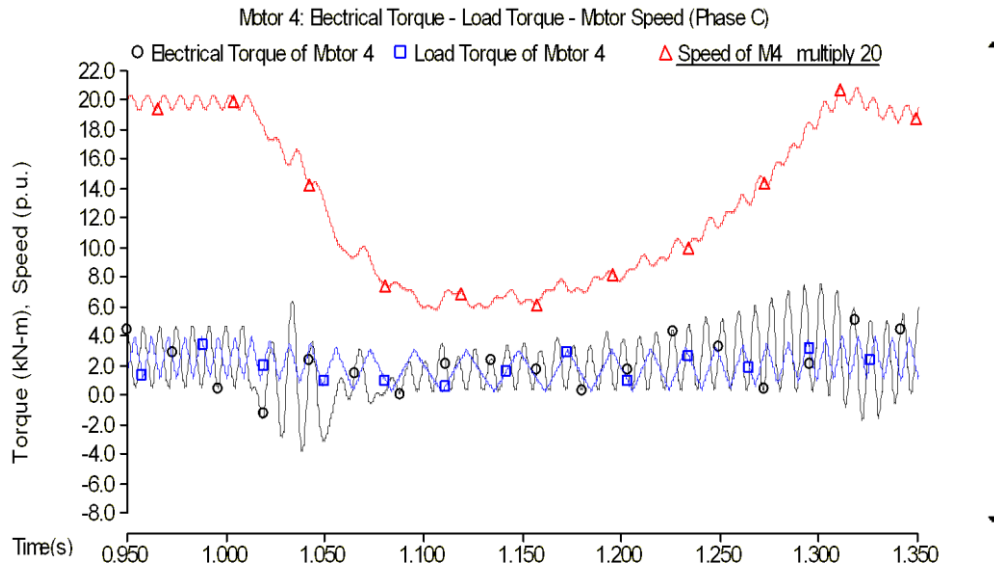
Figure 5.8 Plot of electrical torque and load torque, and scaled speed of motor 4 (Phase-C)

51
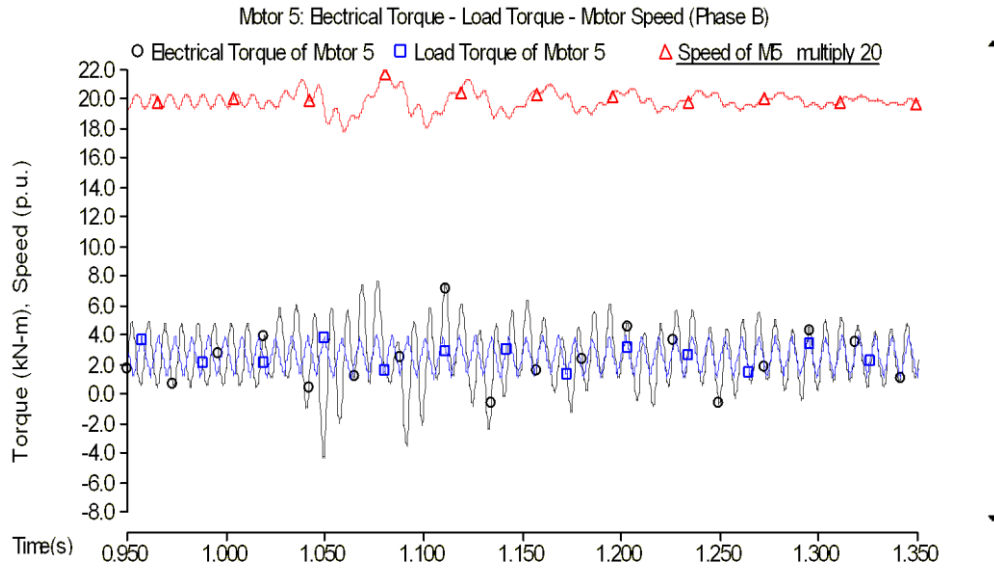
Figure 5.9 Plot of electrical torque and load torque, and scaled speed of motor 5
(Phase-B)
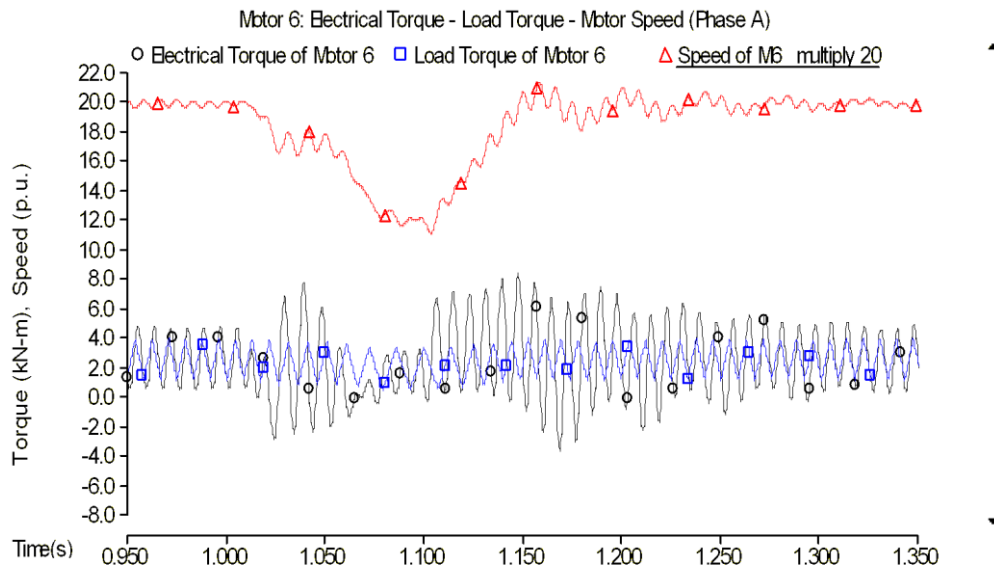
Figure 5.10 Plot of electrical torque and load torque, and scaled speed of motor 6
(Phase-A)
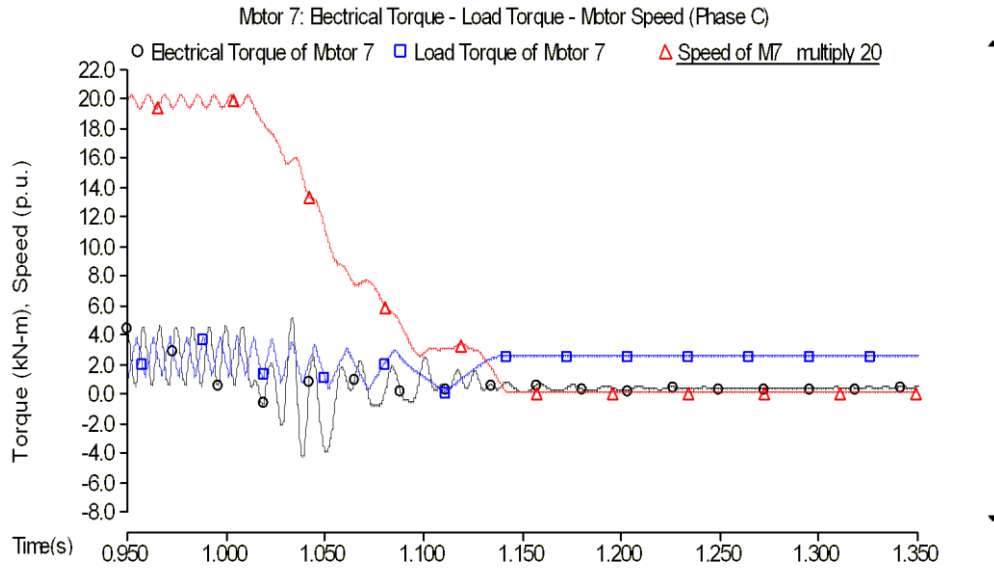
Figure 5.11 Plot of electrical torque and load torque, and scaled speed of motor 7 (Phase-C)
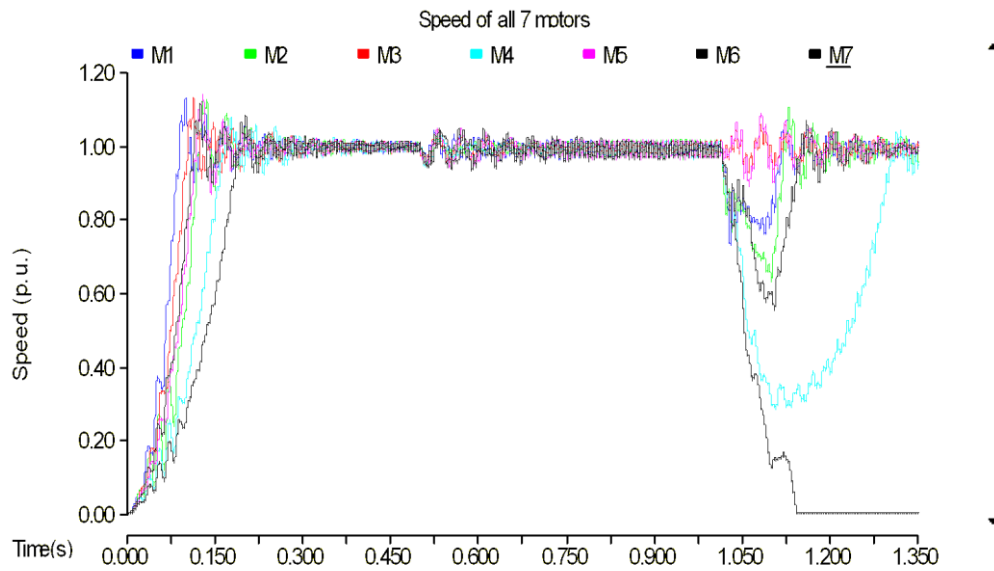
Figure 5.12 Speed plot of all seven motors
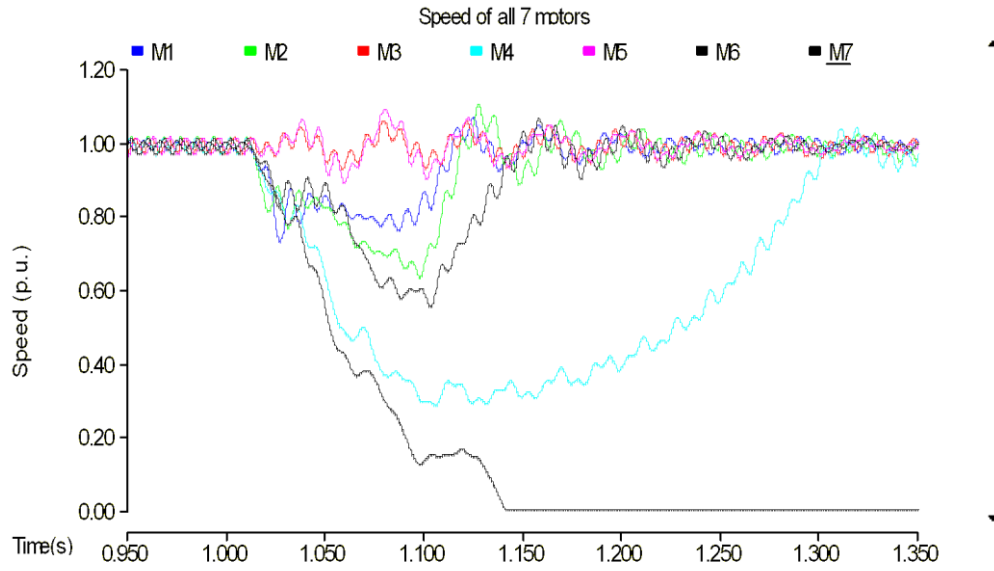
Figure 5.13 Zoomed in speed plot of all 7 motors
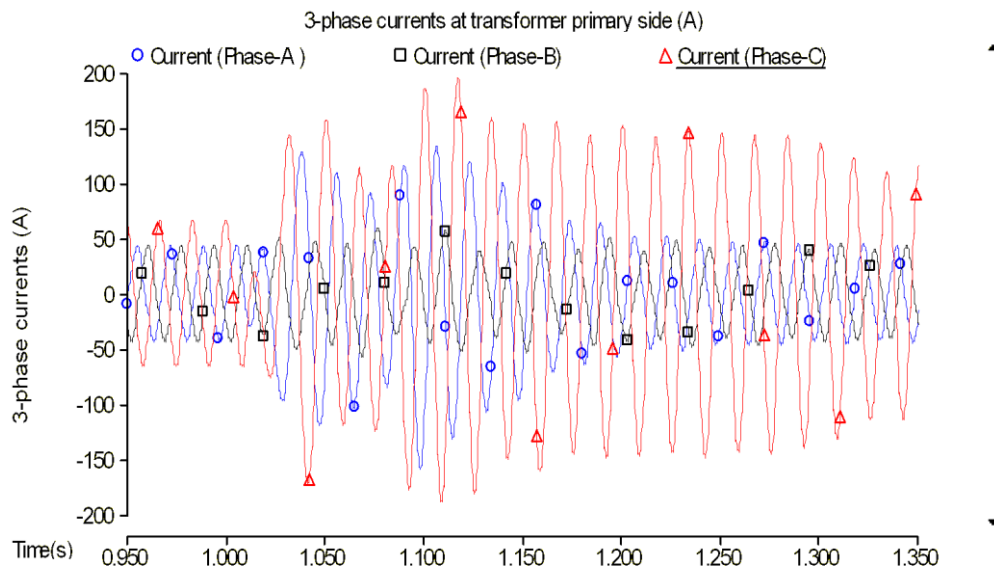
Figure 5.14 Three-phase currents plot at primary side of main transformer

5.3   Analysis of results

When the motor starts running, the start-up current is very high. As a result, the terminal voltage of each motor is lower than normal operation values because of large voltage drop along the feeder induced by large current amplitude. Since motor 7 is at the end of the feeder and most importantly it is at the heavily loaded phase-C, it stalls in this case. It is clearly shown in Figure 5.3 that the terminal voltage of motor 7 after fault clearance is lower than normal condition due to voltage drop induced by big stator current drawn in the stalled mode. It is observed from Figure 5.12 that all 7 motors are driven to start up at the same time, Motor 1 which is on phase-A and closest to the head of feeder accelerates fastest because of the least voltage drop from the head to the node where it is connected. Phase-C is heavily loaded and voltage degradation on phase-C is more severe than A and B phases. Motors coupled to phase-C start up slower than motors on A and B phases. The unbalanced loading on the feeder also illustrates the unbalanced three-phase currents at primary side of main transformer shown in Figure 5.14. Before fault is applied at 1 second, current flowing on phase-C is larger than A and B phases because phase-C is heavily loaded. After the clearance of the voltage depression, the current in phase-C increases to about 2.33 times of its normal value because motor 7 at the tail of feeder stalls and draws high current.

The instantaneous rotor speed is not constant but varies in accordance with the variation of electrical and load torques at twice supply frequency. For each population of motors, the relative phase of electrical torque and load torque at the moment of inception of a supply disturbance is random and depends on the when

the triangular torque is applied. That means two motors on the same phase would behave differently because the developed load torque prior to the voltage dip is not identical. Accordingly, the electrical torque would be different from motor to motor as well. Simply speaking, the motor is susceptible to the phasing of supply voltage, load torque and the fed-in current.

The comparison of electrical torque trajectories in Figure 5.4 through Figure 5.11 reveals that when the voltage disturbance is initialized the excursions of electrical torque are similar. For those motors that do not stall in phase-A and phase-C, the subsequent swings grow strongly positive. The positive component of electrical torque contributes to the reacceleration of motor. On the contrary, the stalled motors increase the negative variations of electrical torque.

Chapter 6. CONCLUSIONS AND FUTURE WORK

6.1 Conclusions

The investigation described above indicates that motor stalling and reacceleration are impacted by multiple factors. The point-on-wave (P-O-W) study in EMTP type simulation tools makes it possible to identify the impact of each influence factor. The "prone-to-stall" motors are susceptible to sudden change in terminal voltage. Motors are more prone to stall when subjected to unacceptable voltage drops. Additionally, the point where the fault is applied on the sinusoidal wave will make a big difference in deciding the post-fault state of motor. Even though the voltage reduces to a very low level, motor may still not stall if this occurs at the peak of the voltage wave. The likelihood that motors will stall is strongly related to their mechanical loading. It is quite possible that stalling of compressor motors does not require a long interval of voltage depression. Moderately loaded motors can stall for dips as short as 5 cycles. The relative phase of electrical and load torque where the voltage disturbance is induced also has correlation with stalling. Positive swings of electrical torque after the clearance of fault are strong contributing factors to propel the motor to recover its speed. The conclusions drawn from the investigation of multiple units of motors connected to a realistic three-phase distribution feeder can be correlated with the simulation results for an individual motor.

6.2   Future work

The model is designed for understanding the real-time characteristics of air-conditioner compressor single phase induction motor. Statistical field data is needed as a basis for further research on this subject. The field test results of motor behavior and voltage profile will be collected and used to examine the dynamic and steady-state response of the designed model in PSCAD and to generalize the rationale of motor stalling in a real-time scenario.

Compared with the expensive RTDS machinery [9], the PSCAD simulator has advantages of price and compactness. PSCAD programs can be installed in tens of computers in a room conveniently where only 2 or 3 sets of RTDS machinery can be placed in the same room. Cooperation is need with Manitoba High Voltage Direct Current (HVDC) research center, the developer of PSCAD, to incorporate the new motor model into PSCAD with good computing efficiency. With their technical support, the user-defined model can be reprogrammed in production form and incorporated into the master library of PSCAD software. It will then be available to the air-conditioner manufacturers and other facility producers for use in analyzing the A/C equipment and supplementary devices.

Application of the newly designed model in simulations of the bulk electric transmission system with several distribution feeder branches will draw engineers' attention for studying the FIDVR phenomenon in the future.

BIBLIOGRAPHY

[1]   B. R. Williams, W. R. Schmus and D. C. Dawson, "Transmission voltage recovery delayed by stalled air-conditioner compressors," *IEEE Transactions on Power Systems,* vol. 7, no. 3, pp. 1173 - 1181, 1992.

[2]   J. W. Shaffer, "Air-conditioner response to transmission faults," *IEEE Transactions on Power Systems,* vol. 12, no. 2, pp. 614 - 621, 1997.

[3]   V. Stewart and E. H. Camm, "Modeling of stalled motor loads for power system short-term voltage stability analysis," in *Power Engineering Society General Meeting*, 2005.

[4]   K. Tomiyama, J. P. Daniel and S. Ihara, "Modeling air-conditioner load for power system studies," *IEEE Transactions on Power Systems,* vol. 13, no. 2, pp. 414 - 421, 1998.

[5]   B. Lesieutre, D. Kosterev and J. Undrill, "Phasor modeling approach for single phase A/C motors," in *Power and Energy Society General Meeting*, Pittsburgh, PA, 2008.

[6]   R. Bravo, R. Yinger, D. Chassin, H. Huang, N. Lu, I. Hiskens and G. Venkataramanan, "Final project report Load modeling transmission research," Lawrence Berkeley National Laboratory, 2010.

[7]   A. M. Stankovic, B. C. Lesieutre and T. Aydin, "Modeling and analysis of single-phase induction machines with dynamic phasors," *IEEE Transactions on Power Systems,* vol. 14, no. 1, pp. 9 - 14, 1999.

[8]   J. Undrill, "Difference equation form of single phase induction motor model," 2011.

[9]   K. G. Ravikumar, "Lawrence Berkeley National Laboratory RTDS Testing Final Report," SEL Engineering Services, 2012.

[10]   P. C. Krause, O. Wasynczuk and S. D. Sudhoff, Analysis of electric machinery and drive systems, Piscataway, NJ: IEEE Press Series on Power Engineering, 2002.

[11] P. C. Krause, "Simulation of unsymmetrical 2-phase induction machines," *IEEE Transactions on Power Apparatus and Systems,* vol. 84, no. 11, pp. 1025 - 1037, 1965.

[12] P. Pourbeik and B. Agrawal, "A hybrid model for representing air-conditioner compressor motor behavior in power system studies," in *Power and Energy Society General Meeting*, Pittsburgh, PA, 2008.

[13] H. C. Stanley, "An analysis of the induction machine," *Transactions of the American Institute of Electrcial Engineers,* vol. 57, no. 12, pp. 751 - 757, 1938.

[14] W. V. Lyon and C. Kingsley, "Analysis of unsymmetrical machines," *Transactions of the American Institute of Electrical Engineers,* vol. 55, no. 5, pp. 471 - 476, 1936.

[15] "WECC MVWG composite load model for dynamic simulations," WECC MVWG, 2012.

[16] "Single Phase Induction Motors," New Age International, [Online]. Available: http://www.newagepublishers.com/samplechapter/001136.pdf.

[17] J. Undrill, Power system dynamics and control, Class Notes, Arizona State University, 2012.

[18] C. T. Chen, Linear system theory and design, New York: Oxford University Press, 1999.

[19] A comprehensive resource for EMTDC, Winnipeg, Manitoba, Canada: Manitoba HVDC Research Centre, 2010.

[20] User's guide on the use of PSCAD, Winnipeg, Manitoba, Canada: Manitoba HVDC Research Centre, 2010.

[21] H. W. Dommel, "Digital computer solution of electro-magnetic transients in single- and multiphase networks," *IEEE Transactions on Power Apparatus and Systems,* Vols. PES-88, no. 4, pp. 388 - 399, 1969.

APPENDIX

FORTRON SOURCE CODE OF MODEL DEFINITION

A.1 Fortran script in 'Branch' segment of component definition

```
! Define two Norton branches as a part of PSCAD electric network

BRNANG=$NA $NG BREAKER 1.0
BRNBNG=$NB $NG BREAKER 1.0
```

A.2 Fortran script in 'Dsdyn' segment of component definition

```
! RTCF is internal storage array used in data initialization

#SUBROUTINE SPIM_EXE Single phase motor model
#SUBROUTINE SPIM_RTC Single phase motor initiating function

#STORAGE RTCF:16
#STORAGE REAL:16

#BEGIN
      #LOCAL REAL TLOADB,TAVB,OMEGAOB
      #LOCAL REAL RSB,RRB,LMUB,LLSB,LLRB
      #LOCAL REAL PSIBB,WR2B,HB
      #LOCAL REAL SCALEB
      #LOCAL REAL NABB,S1B,S12B
      #LOCAL REAL TDLDB

       CALL SPIM_RTC($SS,$BRNANG,$BRNBNG,$Tload,$Scale,&
       $Tav,$Freq,$rs,$rr,&
       $Xmu,$Xls,$Xlr,$Vbase,$Ibase,$nab,$s1,$s12,&
       $Tdld,$Diam,TLOADB,TAVB,OMEGAOB,RSB,RRB,LMUB,LLSB,&
       LLRB,PSIBB,WR2B,HB,SCALEB,NABB,S1B,S12B,TDLDB)

      RTCF(NRTCF)=TLOADB
      RTCF(NRTCF+1)=TAVB
      RTCF(NRTCF+2)=OMEGAOB
      RTCF(NRTCF+3)=RSB
      RTCF(NRTCF+4)=RRB
      RTCF(NRTCF+5)=LMUB
      RTCF(NRTCF+6)=LLSB
      RTCF(NRTCF+7)=LLRB
      RTCF(NRTCF+8)=PSIBB
      RTCF(NRTCF+9)=WR2B
      RTCF(NRTCF+10)=HB
      RTCF(NRTCF+11)=SCALEB
      RTCF(NRTCF+12)=NABB
      RTCF(NRTCF+13)=S1B
      RTCF(NRTCF+14)=S12B
      RTCF(NRTCF+15)=TDLDB

       NRTCF=NRTCF+16

#ENDBEGIN

      #LOCAL REAL TLOAD,TAV,OMEGAO
      #LOCAL REAL RS,RR,LMU,LLS,LLR
      #LOCAL REAL PSIB,WR2,H
      #LOCAL REAL SCALE
      #LOCAL REAL NAB,S1,S12
      #LOCAL REAL TDLD

      TLOAD=RTCF(NRTCF)
      TAV=RTCF(NRTCF+1)
      OMEGAO=RTCF(NRTCF+2)
      RS=RTCF(NRTCF+3)
      RR=RTCF(NRTCF+4)
      LMU=RTCF(NRTCF+5)
      LLS=RTCF(NRTCF+6)
      LLR=RTCF(NRTCF+7)
      PSIB=RTCF(NRTCF+8)
```

```
      WR2=RTCF(NRTCF+9)
      H=RTCF(NRTCF+10)
      SCALE=RTCF(NRTCF+11)
      NAB=RTCF(NRTCF+12)
      S1=RTCF(NRTCF+13)
      S12=RTCF(NRTCF+14)
      TDLD=RTCF(NRTCF+15)

       NRTCF=NRTCF+16

#STORAGE REAL:16
#STORAGE INTEGER:1
#LOCAL INTEGER IDV


       IDV=NSTORF

       CALL SPIM_EXE($SS,$NA,$NB,$NG,$BRNANG,$BRNBNG,TLOAD,TAV,OMEGAO,RS,&
        RR,LMU,LLS,LLR,PSIB,WR2,H,SCALE,NAB,S1,&
        S12,TDLD)

       NSTORF=NSTORF+16

#OUTPUT REAL Rspeed {STORF(IDV+4)/377.0}
#OUTPUT REAL Imainst {STORF(IDV+10)/1000.0}
#OUTPUT REAL Iauxst {STORF(IDV+11)/1000.0}
#OUTPUT REAL Telectrical {STORF(IDV+14)/1000.0}
#OUTPUT REAL Tldout {STORF(IDV+15)/1000.0}
#OUTPUT REAL V {STORF(IDV+5)}
#OUTPUT REAL SA {STORF(IDV+6)}
#OUTPUT REAL flexible {STORF(IDV+7)}
```

A.3 Source code of external subroutines

A.3.1 Source code of subroutine 'SPIM_RTC'

```
! RTCF is internal storage array used in data initialization
! CURRENT_SOURCE2_CFG is EMTDC subroutine to initialize Norton current source

!*****************************************
      SUBROUTINE SPIM_RTC(SS,BRNANG,BRNBNG,TloadBB,ScaleBB,TavBB,FreqBB,&
       rsBB,rrBB,XmuBB,XlsBB,XlrBB,VbaseBB,IbaseBB,&
       nabBB,s1BB,s12BB,TdldBB,DiamBB,TLOADB,TAVB,OMEGAOB,&
       RSB,RRB,LMUB,LLSB,LLRB,PSIBB,WR2B,HB,SCALEB,&
       NABB,S1B,S12B,TDLDB)

       INCLUDE 'nd.h'
       INCLUDE 'emtstor.h'
       INCLUDE 'rtconfig.h'
       INCLUDE 's1.h'
       INCLUDE 'emtconst.h'
       INCLUDE 's0.h'
       INCLUDE 'branches.h'

      INTEGER SS,BRNANG, BRNBNG

      REAL TloadBB,TavBB,FreqBB
      REAL rsBB,rrBB,XmuBB,XlsBB,XlrBB
      REAL VbaseBB,IbaseBB
      REAL ScaleBB
      REAL nabBB,s1BB,s12BB
      REAL TdldBB
      REAL DiamBB

      REAL TLOADB,TAVB,OMEGAOB
      REAL RSB,RRB,LMUB,LLSB,LLRB
```

```
      REAL PSIBB,WR2B,HB
      REAL SCALEB
      REAL NABB,S1B,S12B,TDLDB

       TLOADB=TloadBB*ScaleBB
       TAVB=TavBB*ScaleBB
       OMEGAOB=2*3.14159265*FreqBB
       RSB=rsBB/ScaleBB
       RRB=rrBB/ScaleBB
       LMUB=(XmuBB/OMEGAOB)/ScaleBB
       LLSB=(XlsBB/OMEGAOB)/ScaleBB
       LLRB=(XlrBB/OMEGAOB)/ScaleBB
       PSIBB=(1.414*VbaseBB)/OMEGAOB
       WR2B=7800*(3.14159265/32)*0.2*(DiamBB**4)*ScaleBB
       HB=0.5*WR2B*(OMEGAOB**2)/(4500*ScaleBB)
       SCALEB=ScaleBB
       NABB=nabBB
       S1B=s1BB
       S12B=s12BB
       TDLDB=TdldBB

       CALL CURRENT_SOURCE2_CFG(BRNANG,SS)
       CALL CURRENT_SOURCE2_CFG(BRNBNG,SS)

      END SUBROUTINE SPIM_RTC
```

A.3.2 Source code of subroutine 'SPIM_EXE'

```
! RTCF is internal storage array used in data initialization.
! STORF is internal storage array used to iteratively save dynamic variables in
each time instant.
! CURRENT_SOURCE2_EXE is EMTDC subroutine to specify the values of Norton
admittance and current source at each time step.
! VDC is a command to extract the resolved voltage from electric network.
! SESAT is saturation function.

!****************************************
      SUBROUTINE SPIM_EXE(SS,NA,NB,NG,BRNANG,BRNBNG,TLOAD,TAV,&
       OMEGAO,RS,RR,LMU,LLS,LLR,PSIB,WR2,H,SCALE,NAB,S1,S12,TDLD)

      INCLUDE 'nd.h'
      INCLUDE 'emtstor.h'
      INCLUDE 'rtconfig.h'
      INCLUDE 's1.h'
      INCLUDE 'emtconst.h'
      INCLUDE 's0.h'
       INCLUDE 'branches.h'


! DEFINE INPUT
      INTEGER SS,NA,NB,NG,BRNANG,BRNBNG

      REAL TLOAD,TAV,OMEGAO
      REAL RS,RR,LMU,LLS,LLR
      REAL PSIB,WR2,H
      REAL SCALE
      REAL NAB,S1,S12
      REAL TDLD


! DEFINE LOCAL VARIABLE

      REAL LL(4,4)
      REAL LZ(4,4)
      REAL LMAT(4,4)
      REAL VMC(4)
      REAL IMC(4)
      REAL PMC(4)
```

64

```fortran
      REAL Z(4,4), ZSS(2,2), ZSR(2,2), ZRS(2,2)
      REAL ZRR(2,2), INVZRR(2,2), VT(4), VTS(2)
      REAL VTR(2), ZSRINVZRR(2,2), ZZZ(2,2)
      REAL ZTH(2,2), ETH(2), VRR(2), IS(2), IR(2)

      REAL DETRR
      REAL VTHB

      REAL VAS, VBS, VAR, VBR
      REAL PAS, PBS, PAR, PBR
      REAL IAS, IBS, IAR, IBR
      REAL VTH, VAMP
      REAL PAM, PBM
      REAL TE, A, AA, AAA, AAAA, ANGLE, SPEED,TLA
      REAL V, SA, SB, RCAGE
      REAL STROKE, TWOSTR
      REAL PHAME

      REAL FLEX

      INTEGER I, J

       PHAME=3.14159265

      IF(TIMEZERO) THEN

        STORF(NSTORF)=0.0
        STORF(NSTORF+1)=0.0
        STORF(NSTORF+2)=0.0
        STORF(NSTORF+3)=0.0
        STORF(NSTORF+4)=0.0
        STORF(NSTORF+5)=0.0
        STORF(NSTORF+6)=0.0
        STORF(NSTORF+7)=0.0
        STORF(NSTORF+8)=0.0
        STORF(NSTORF+9)=0.0
        STORF(NSTORF+10)=0.0
        STORF(NSTORF+11)=0.0
        STORF(NSTORF+12)=0.0
        STORF(NSTORF+13)=0.0
        STORF(NSTORF+14)=0.0
        STORF(NSTORF+15)=0.0

      END IF

! Extract the old value from storage Array

      VTH=STORF(NSTORF)
      VAS=STORF(NSTORF+1)
      VBS=STORF(NSTORF+2)
      ANGLE=STORF(NSTORF+3)
      SPEED=STORF(NSTORF+4)
      V=STORF(NSTORF+5)
      SA=STORF(NSTORF+6)
      FLEX=STORF(NSTORF+7)
      PAS=STORF(NSTORF+8)
      PBS=STORF(NSTORF+9)
      IMC(1)=STORF(NSTORF+10)
      IMC(2)=STORF(NSTORF+11)
      IMC(3)=STORF(NSTORF+12)
      IMC(4)=STORF(NSTORF+13)
      TE=STORF(NSTORF+14)
      TLA=STORF(NSTORF+15)

! Calculate the new value using the old ones, main body of the subroutine

      VTH=(VDC(NA,SS)-VDC(NG,SS))*1000.0
      VTHB=(VDC(NB,SS)-VDC(NG,SS))*1000.0
```

```fortran
        AA=ANGLE
        V=SQRT(PAS**2+PBS**2)/PSIB

        SA=1.0+SESAT(V,S1,S12)*V
        SB=SA


! Compute SA and SB

        LL(1,1)=(LMU+LLS)/SA
        LL(2,1)=0.0
        LL(3,1)=(LMU/SA)*COS(AA)
        LL(4,1)=(LMU/SB)*SIN(AA)
        LL(1,2)=0.0
        LL(2,2)=(LMU*(NAB**2)+LLS*(NAB**2))/SB
        LL(3,2)=-(LMU/SA)*SIN(AA)*NAB
        LL(4,2)=(LMU/SB)*COS(AA)*NAB
        LL(1,3)=(LMU/SA)*COS(AA)
        LL(2,3)=-(LMU/SB)*SIN(AA)*NAB
        LL(3,3)=(LMU+LLR)/SA
        LL(4,3)=0.0
        LL(1,4)=(LMU/SA)*SIN(AA)
        LL(2,4)=(LMU/SB)*COS(AA)*NAB
        LL(3,4)=0.0
        LL(4,4)=(LMU+LLR)/SB

        LZ(1,1)=0.0
        LZ(2,1)=0.0
        LZ(3,1)=-SPEED*(LMU/SA)*SIN(AA)
        LZ(4,1)=SPEED*(LMU/SB)*COS(AA)
        LZ(1,2)=0.0
        LZ(2,2)=0.0
        LZ(3,2)=-SPEED*(LMU/SA)*COS(AA)*NAB
        LZ(4,2)=-SPEED*(LMU/SB)*SIN(AA)*NAB
        LZ(1,3)=-SPEED*(LMU/SA)*SIN(AA)
        LZ(2,3)=-SPEED*(LMU/SB)*COS(AA)*NAB
        LZ(3,3)=0.0
        LZ(4,3)=0.0
        LZ(1,4)=SPEED*(LMU/SA)*COS(AA)
        LZ(2,4)=-SPEED*(LMU/SB)*SIN(AA)*NAB
        LZ(3,4)=0.0
        LZ(4,4)=0.0

        IF (SPEED < OMEGAO) THEN
            RCAGE=RR*(5.0-4.0*SPEED/OMEGAO)
        ELSE
            RCAGE=RR
        END IF

        DO I=1,4
          DO J=1,4
            LMAT(I,J)=LL(I,J)+DELT*LZ(I,J)
          END DO
        END DO

        LMAT(1,1)=LMAT(1,1)+DELT*RS
        LMAT(2,2)=LMAT(2,2)+DELT*RS
        LMAT(3,3)=LMAT(3,3)+DELT*RCAGE
        LMAT(4,4)=LMAT(4,4)+DELT*RCAGE

! Zth and Eth calculation

        DO I=1,4
          DO J=1,4
            Z(I,J)=LMAT(I,J)/DELT
          END DO
        END DO
```

```
DO I=1,4
  VT(I)=0.0
    DO J=1,4
      VT(I)=VT(I)-LL(I,J)/DELT*IMC(J)
    END DO
END DO

VTS(1)=VT(1)
VTS(2)=VT(2)
VTR(1)=VT(3)
VTR(2)=VT(4)

ZSS(1,1)=Z(1,1)
ZSS(1,2)=Z(1,2)
ZSS(2,1)=Z(2,1)
ZSS(2,2)=Z(2,2)
ZSR(1,1)=Z(1,3)
ZSR(1,2)=Z(1,4)
ZSR(2,1)=Z(2,3)
ZSR(2,2)=Z(2,4)
ZRS(1,1)=Z(3,1)
ZRS(1,2)=Z(3,2)
ZRS(2,1)=Z(4,1)
ZRS(2,2)=Z(4,2)
ZRR(1,1)=Z(3,3)
ZRR(1,2)=Z(3,4)
ZRR(2,1)=Z(4,3)
ZRR(2,2)=Z(4,4)

DETRR=ZRR(1,1)*ZRR(2,2)-ZRR(1,2)*ZRR(2,1)

INVZRR(1,1)=ZRR(2,2)/DETRR
INVZRR(1,2)=-ZRR(1,2)/DETRR
INVZRR(2,1)=-ZRR(2,1)/DETRR
INVZRR(2,2)=ZRR(1,1)/DETRR

DO I=1,2
  DO J=1,2
    ZSRINVZRR(I,J)=0.0
  END DO
END DO

DO I=1,2
  DO J=1,2
    DO K=1,2
      ZSRINVZRR(I,J)=ZSRINVZRR(I,J)+ZSR(I,K)*INVZRR(K,J)
    END DO
  END DO
END DO


DO I=1,2
  DO J=1,2
    ZZZ(I,J)=0.0
  END DO
END DO


DO I=1,2
  DO J=1,2
    DO K=1,2
      ZZZ(I,J)=ZZZ(I,J)+ZSRINVZRR(I,K)*ZRS(K,J)
    END DO
  END DO
END DO


DO I=1,2
  DO J=1,2
    ZTH(I,J)=ZSS(I,J)-ZZZ(I,J)
```

```
      END DO
    END DO


    DO I=1,2
      ETH(I)=0.0
        DO J=1,2
          ETH(I)=ETH(I)-ZSRINVZRR(I,J)*VTR(J)
        END DO
    END DO


    DO I=1,2
      ETH(I)=ETH(I)+VTS(I)
    END DO

    IAS=(VTH-ETH(1))/ZTH(1,1)
    IBS=(VTHB-ETH(2))/ZTH(2,2)

    CALL CURRENT_SOURCE2_EXE(BRNANG,SS,1.0/ZTH(1,1),(IAS-
VTH/ZTH(1,1))/1000.0)
    CALL CURRENT_SOURCE2_EXE(BRNBNG,SS,1.0/ZTH(2,2),(IBS-
VTHB/ZTH(2,2))/1000.0)

    FLEX=ETH(2)/1000.0


    IS(1)=IAS
    IS(2)=IBS


    DO I=1,2
      VRR(I)=0.0
        DO J=1,2
          VRR(I)=VRR(I)+ZRS(I,J)*IS(J)
        END DO
    END DO


    DO I=1,2
      VRR(I)=VRR(I)+VTR(I)
    END DO


    DO I=1,2
      IR(I)=0.0
        DO J=1,2
          IR(I)=IR(I)-INVZRR(I,J)*VRR(J)
        END DO
    END DO

    IAR=IR(1)
    IBR=IR(2)

    IMC(1)=IAS
    IMC(2)=IBS
    IMC(3)=IAR
    IMC(4)=IBR


    DO I=1,4
      PMC(I)=0.0
      DO J=1,4
      PMC(I)=PMC(I)+LL(I,J)*IMC(J)
      END DO
    END DO

    PAS=PMC(1)
    PBS=PMC(2)
```

68

```
        PAM=PAS-(LLS/SA)*IAS
        PBM=PBS-NAB*NAB*(LLS/SB)*IBS

!!!!!!!!!!!!!!!!!!!!!!!!!!!!!!!!!!!!!!!!!!!!!!!!!!!!!!!!!!!!!!

        TE=PAM*(-IAR*SIN(AA)+IBR*COS(AA))-PBM*(IBR*SIN(AA)+IAR*COS(AA))

! Model the load

        IF(TIME >= TDLD) THEN
          STROKE=3.14159265/2.0
          TWOSTR=2.0*STROKE
          AAA=MOD((ANGLE+PHAME),STROKE)
          IF(MOD((ANGLE+PHAME),TWOSTR)<STROKE) THEN
              AAAA=TAV+TAV*(AAA-STROKE/2.0)*2.0/STROKE
          ELSE
              AAAA=-TAV+TAV*(3.0*STROKE/2.0-AAA)*2.0/STROKE
          END IF
        ELSE
          AAAA=0.0
        END IF

        TLA=(SPEED/OMEGAO)*(SPEED/OMEGAO)*TLOAD+AAAA

        IF(SPEED < 0.0) THEN
          SPEED=0.0
        END IF

          SPEED=SPEED+DELT*(TE-TLA)/WR2
          ANGLE=ANGLE+SPEED*DELT
          ANGLE=MOD(ANGLE,6.2831853)


          STORF(NSTORF)=VTH
          STORF(NSTORF+1)=VAS
          STORF(NSTORF+2)=VBS
          STORF(NSTORF+3)=ANGLE
          STORF(NSTORF+4)=SPEED
          STORF(NSTORF+5)=V
          STORF(NSTORF+6)=SA
          STORF(NSTORF+7)=FLEX
          STORF(NSTORF+8)=PAS
          STORF(NSTORF+9)=PBS
          STORF(NSTORF+10)=IMC(1)
          STORF(NSTORF+11)=IMC(2)
          STORF(NSTORF+12)=IMC(3)
          STORF(NSTORF+13)=IMC(4)
          STORF(NSTORF+14)=TE
          STORF(NSTORF+15)=TLA

      END SUBROUTINE SPIM_EXE
```

A.3.3 Source code of saturation function 'SESAT'

```
!*****************************************
      REAL FUNCTION SESAT(PSI_R,S1_R,S12_R)


        REAL PSI_R,S1_R,S12_R
        REAL A_R,B_R

        A_R=SQRT(S12_R/S1_R)
        B_R=(1.2-A_R)/(1.0-A_R)
        A_R=S12_R/((1.2-B_R)*(1.2-B_R))

        IF(PSI_R>B_R) THEN
          SESAT=A_R*(PSI_R-B_R)*(PSI_R-B_R)
```

```
      ELSE
        SESAT=0.0
      END IF

  END FUNCTION SESAT
```